Multi-omics characterization of partial chemical reprogramming reveals evidence of cell rejuvenation

Wayne Mitchell[1], Ludger J.E. Goeminne[1], Alexander Tyshkovskiy[1], Sirui Zhang[1], Joao A. Paulo[2], Kerry A. Pierce[3], Angelina H. Choy[3], Clary B. Clish[3], Steven P. Gygi[2], and Vadim N. Gladyshev[1*]

[1]Division of Genetics, Department of Medicine, Brigham and Women's Hospital, Harvard Medical School, Boston, MA 02115 United States

[2]Department of Cell Biology, Harvard Medical School, Boston, MA 02115 United States

[3]Broad Institute of MIT and Harvard, Cambridge, MA 01241 United States

*Corresponding Author

Dr. Vadim N. Gladyshev

77 Avenue Louis Pasteur

Boston, MA 02115

e-mail: vgladyshev@rics.bwh.harvard.edu

ABSTRACT

Partial reprogramming by cyclic short-term expression of Yamanaka factors holds promise for shifting cells to younger states and consequently delaying the onset of many diseases of aging. However, the delivery of transgenes and potential risk of teratoma formation present challenges for *in vivo* applications. Recent advances include the use of cocktails of compounds to reprogram somatic cells, but the characteristics and mechanisms of partial cellular reprogramming by chemicals remain unclear. Here, we report a multi-omics characterization of partial chemical reprogramming in fibroblasts from young and aged mice. We measured the effects of partial chemical reprogramming on the epigenome, transcriptome, proteome, phosphoproteome, and metabolome. At the transcriptome, proteome, and phosphoproteome levels, we saw widescale changes induced by this treatment, with the most notable signature being an upregulation of mitochondrial oxidative phosphorylation. Furthermore, at the metabolome level, we observed a reduction in the accumulation of aging-related metabolites. Using both transcriptomic and epigenetic clock-based analyses, we show that partial chemical reprogramming reduces the biological age of mouse fibroblasts. We demonstrate that these changes have functional impacts, as evidenced by changes in cellular respiration and mitochondrial membrane potential. Taken together, these results illuminate the potential for chemical reprogramming reagents to rejuvenate aged biological systems, and warrant further investigation into adapting these approaches for *in vivo* age reversal.

INTRODUCTION

Cellular aging is accompanied by various features, such as epigenetic changes, upregulation of inflammation, metabolic dysfunction, decreased proteostatic clearance, and increased DNA damage[1-5]. However, while all these hallmarks consistently show changes during aging, there are only limited insights into their potential causative roles. Additionally, many therapies that have targeted single 'hallmarks' of aging have failed to increase lifespan or improve biological functions *in vivo*[6,7]. An alternative way to discover therapies for targeting biological age is to develop tools to quantify it, and then screen interventions for their effect on biological age reduction. Several methods currently exist for quantifying cell aging, such as epigenetic clocks that use mean methylation levels of CpG sites that change during aging[8], transcriptomic clocks that rely on age-associated changes in gene expression[9,10], telomere clocks that rely on age-dependent attrition[11], and various proteomic, metabolomic, and glycomic clocks[12-15]. Most notably, 2nd generation epigenetic clocks trained to predict phenotypic measures and mortality instead of chronological age have been shown to outperform many of these aforementioned clocks in their ability to predict lifespan and healthspan[16].

Using various methods for biological age prediction, several intervention strategies have been recently shown to slow and/or reverse biological aging. These include pharmacological interventions such as rapamycin and metformin[17-20], genetic interventions[21], heterochronic parabiosis[22,23], and partial reprogramming by doxycycline-induced expression of Yamanaka factors[24-26]. A natural rejuvenation process during early development has also been described[27,28]. While partial reprogramming of somatic cells has been shown to lead to improvements in biological function lost during aging[29,30], the effective *in vivo* delivery of the transgenic cassettes and precise control of the expression of Yamanaka factors present challenges. To date, no peer-reviewed studies have demonstrated lifespan increase of wild type animals upon the treatment.

Recently, administration of cocktails of small-molecule compounds have been shown to reprogram somatic cells back to pluripotency[31,32]; moreover, short-term administration of two chemical cocktails (7c and 2c) have demonstrated efficacy at ameliorating several hallmarks of aging in human fibroblasts, while simultaneously preserving cellular identity[33]. Thus, partial reprogramming by short-term administration of chemicals could represent a more feasible, controllable, and adaptable method for inducing rejuvenation *in vivo.* However, the effects of short-term chemical reprogramming on biological age and function are currently unknown, and the mechanisms by which these chemical reprogramming cocktails act are not fully elucidated.

To address this knowledge gap, we have studied the effects of short-term partial cellular reprogramming by chemicals in both young and aged mouse fibroblasts using a multi-tiered

approach. In essence, we have systematically evaluated the impact of chemical reprogramming on (i) the epigenome, transcriptome, proteome, phosphoproteome, and metabolome using various omics-based approaches, (ii) biological age with epigenetic and transcriptomic clocks, and (iii) cellular function using gene set enrichment analyses (GSEA) and measurements of cellular respiration. We demonstrate that partial chemical reprogramming induces widespread molecular changes that occur irrespective of the age of the cells. Moreover, we find significant upregulation of mitochondrial OXPHOS complexes in all treatment conditions at the transcriptome and proteome levels. Importantly, mitochondrial OXPHOS is downregulated in aging, and conversely upregulated by many lifespan-increasing interventions. Using both epigenetic and transcriptomic clocks, we show that 7c, but not 2c, reduces biological age in both young and old fibroblasts. Finally, we show that upregulation of mitochondrial OXPHOS by short-term 7c treatment strongly increases spare respiratory capacity and basal mitochondrial transmembrane potential levels. Taken together, these results imply that partial chemical reprogramming by 7c can rejuvenate several aspects of cellular aging, and that regulation of mitochondrial OXPHOS may play an important role in aging and rejuvenation.

MATERIALS AND METHODS

Materials and animals

Young (4-month-old) and old (20-month-old) male C57BL/6 mice were acquired from the NIA aged rodent colonies (Charles River Laboratories, Wilmington, MA) and were fed standard 5053 chow. HEK293T cells were acquired from ATCC (Manassas, VA) and were verified by PCR to be free of mycoplasma contamination. Cell culture reagents were acquired from ThermoFisher Scientific (Waltham, MA), reagents for isolating DNA and RNA were from Qiagen (Hilden, Germany) and Zymo Research (Irvine, CA), respectively, and general preparatory chemicals and reagents were from Sigma-Aldrich (St. Louis, MO). Chemical reprogramming reagents were obtained from the following suppliers: Sigma-Aldrich (repsox, trans-2-Phenylcyclopropylamine, DZNep), Cayman Chemical Company (TTNPB, CHIR99021), Tocris Bioscience (forskolin), and STEMCELL Technologies (valproic acid). Tetramethylrhodamine, methyl ester perchlorate (TMRM) was obtained from MedChem Express (Monmouth Junction, NJ). Antibodies were obtained from Abcam (Cambridge, United Kingdom). All experiments using mice were performed in accordance with institutional guidelines for the use of laboratory animals and were approved by the Brigham and Women's Hospital and Harvard Medical School Institutional Animal Care and Use Committees.

Isolation of mouse fibroblasts

Fibroblasts were isolated from the ears and tails of male C57BL/6 mice according to a published procedure[34]. In brief, mice were euthanized by exposure to CO_2 and cervical dislocation, after which ears and 5 cm of tail were sterilized in 70% ethanol for 5 minutes. After air drying, tissues were cut into small, ~3 mm pieces and digested with a mixture of collagenase and pronase for 90 minutes at 37°C with gentle shaking. Following enzymatic digestion, the tissues were ground in 70 µm cell strainers using a 10 ml syringe plunger, and the resulting cell suspension was centrifuged at 500xg for 5 minutes at room temperature. The cell pellet was resuspended in fresh fibroblast culture media (DMEM/F12, 10% FBS, 1X antibiotic-antimycotic, 50 µM β-mercaptoethanol, 1X non-essential amino acids), spun once more at 500xg, resuspended in 10 ml fibroblast culture media, plated in 10 cm tissue culture dishes, and incubated for 3 days at 37°C, 5% CO_2, and 3% O_2. Following 3 days of incubation, media was replaced to get rid of cellular debris, and the cells were then incubated further until reaching ~80% confluency. Upon reaching the desired confluency, ear and tail fibroblasts were trypsinized and frozen at 1 million cells per cryovial in fibroblast freezing media (fibroblast culture media with 50% FBS and 10% DMSO).

Production of lentivirus

HEK293T cells were cultured in high glucose DMEM plus sodium pyruvate, GlutaMAX, 10% FBS, and 1X antibiotic-antimycotic, and were grown to ~70% confluency at 37°C, 5% CO_2. Viral vectors VSVG and gag/pol 8.91, along with either the polycistronic OSKM cassette[35] (Addgene #20328) or the reverse tetracycline transactivator[36] (Addgene #20342), were encapsulated in PureFection nanoparticles (System Biosciences, Palo Alto, CA) and added drop-by-drop to the culturing cells. After 48 and 72 hours, the cell culture media was collected through a 0.45 um filter, spun at 3,000 RPM for 15 minutes at room temperature, and the resulting supernatant was aliquoted and stored at -80°C.

OSKM reprogramming of fibroblasts

Fibroblasts were seeded in 6-well plates at a cell density of 100,000 cells per well in fibroblast culture media and were incubated for 24 hours at 37°C, 5% CO_2, 3% O_2. Fibroblasts were subsequently co-transfected with 1 ml of each lentivirus (OSKM and reverse tetracycline transactivator), 8 µg/ml polybrene, and 1 ml fresh fibroblast culture media for 3-4 days. Following 3-4 days of transfection, cells were trypsinized and plated on Geltrex® (ThermoFisher, Waltham, MA) coated dishes and incubated for 48 hours. Then, the media was aspirated and replaced with

ES media (fibroblast culture media with 20% FBS, 1000 U/ml mouse Leukemia Inhibitory Factor (LIF), and 2 µg/ml doxycycline) and the cells were cultured for 1-2 weeks until colonies appeared (media replaced every 3 days). Colonies were then manually picked, trypsinized, and plated in Geltrex® coated 24-well plates in N2B27 (1:1 mixture of DMEM/F12: 1X N2 supplement, 7.5% BSA, 1X non-essential amino acids, 100 µM β-mercaptoethanol, 1X antibiotic-antimycotic, and Neurobasal: 1X B27 supplement, 7.5% BSA, 1X non-essential amino acids, 1X GlutaMAX, 100 µM β-mercaptoethanol, 1X antibiotic-antimycotic) media, plus 1 µM PD0325901, 3 µM CHIR99021, 0.5 µM Stemolecule™ A83-01, 1000 U/ml LIF, and 2 µg/ml doxycycline. Colonies that survived in this media were deemed to be fully reprogrammed iPSCs and were further propagated into Geltrex® coated 10 cm dishes and cryofrozen in 50% N2B27 media (without inhibitors or doxycycline), 40% FBS, and 10% DMSO at a cell density of 2 million cells per vial.

AP staining

Fibroblasts were seeded at a density of 100,000 cells per well in 6-well plates, and cells were treated with the specified compounds for 4 or 6 days at 37°C, 5% CO_2, 3% O_2 (media and treatments replenished every 3 days). Cells were washed twice with PBS-T, fixed, and stained with the Stemgent AP Staining Kit II according to the manufacturer's protocol (ReproCELL USA, Inc. Beltsville, MD). Cells were then imaged under a brightfield microscope.

Membrane potential staining

Fibroblasts were stained with 250 nM TMRM and 10 µg/ml Hoescht 33342 in fibroblast culture media for 20 minutes at 37°C, 5% CO_2, and 3% O_2. Then, the media was aspirated, and fibroblasts were washed three times with PBS before imaging in the dark on an AXIO Observer.Z1 (Zeiss, Oberkochen, Baden-Württemberg, Germany). As a positive control, cells were pre-treated with 50 µM of carbonyl cyanide m-chlorophenylhydrazone (CCCP) for 15 minutes prior to incubation with TMRM. Images taken from random fields (4-5 images per treatment condition per biological replicate) were background-subtracted in ImageJ[37], and mean fluorescence was normalized to the number of nuclei per field.

Immunocytochemistry

Cells in 24-well plates were rinsed twice with PBS, fixed in 4% paraformaldehyde for 20 minutes at room temperature, and rinsed twice more with PBS. Then, cells were permeabilized with 0.3% Triton X-100 in PBS for 5 minutes, followed by blocking with 3% BSA for 1 hour at room temperature with gentle shaking. After this, cells were incubated with the indicated primary

antibody overnight at 4°C, rinsed in the morning with PBS for 2 cycles (10 minutes each), and incubated with fluorophore-conjugated secondary antibody for 1 hour at room temperature in the dark. Cells were then finally stained with 10 µg/ml Hoescht 333342 for 10 minutes, rinsed 3 times with PBS, and imaged on an AXIO Observer.Z1 inverted fluorescence microscope (Zeiss, Oberkochen, Baden-Württemberg, Germany).

DNA methylation

DNA was isolated from cells using the DNeasy Blood and Tissue kit according to the manufacturer's instructions (Qiagen, Hilden, Germany). Concentration of DNA samples was measured using the Qubit dsDNA BR kit (Invitrogen, Waltham, MA). DNAmAge (using various epigenetic clocks) was assessed using DNA methylation data obtained on the Horvath mammal 320k array[38] through the Epigenetic Clock Development Foundation (Torrance, CA).

RNA-seq

Fibroblasts were seeded in 6-well plates at a cell density of 100,000 cells per well in fibroblast culture media and were incubated for 6 days at 37°C, 5% CO_2, 3% O_2 with their respective chemical treatments (media replaced once after 3 days). On the 6th day, media was aspirated, and the cells were washed twice with PBS. Then, the cells were directly lysed with 700 µl of Trizol, diluted 1:1 with 200 proof ethanol, and total RNA was isolated using a direct-zol mini prep kit (Zymo Research, Irvine, CA). RNA concentration was measured by Qubit using the RNA HS assay kit (ThermoFisher, Waltham, MA). Libraries were prepared with TruSeq Stranded mRNA LT Sample Prep Kit according to TruSeq Stranded mRNA Sample Preparation Guide, Part # 15031047 Rev. E. Libraries were quantified using the Bioanalyzer (Agilent) and sequenced with Illumina NovaSeq6000 S4 (2×150bp) (reads trimmed to 2×100bp) to get 20M read depth coverage per sample. The BCL (binary base calls) files were converted into FASTQ using the Illumina package bcl2fastq. Fastq files were mapped to the mm10 (GRCm38.p6) mouse genome, and gene counts were obtained with STAR v2.7.2b[39]. Statistical analyses for gene expression were performed with custom models from *DEseq2*[40] 3.13 and *edgeR*[41] 3.34.1 in R. We filtered out genes with low number of reads, keeping only the genes with at least 5 reads in at least 20% of the samples, which resulted in 16,728 detected genes according to Entrez annotation. Filtered data was then passed to RLE normalization. Differential expression of genes perturbed by compounds was analyzed using *edgeR*. Obtained p-values were adjusted for multiple comparison with the Benjamini-Hochberg method.

Association with gene expression signatures of aging and OSKM reprogramming

Association of gene expression log-fold changes induced by chemical reprogramming cocktails with established transcriptomic signatures of aging and OSKM reprogramming was examined with GSEA-based method as described previously[42]. The utilized signatures of aging included tissue-specific liver, kidney, and brain signatures as well as multi-tissue signatures of the mouse, rat, and human[43]. Signatures of OSKM reprogramming included genes differentially expressed during cellular reprogramming of mouse fibroblasts (Mouse), and shared transcriptomic changes during OSKM-induced reprogramming of mouse and human fibroblasts (Mouse & Human)[26]. Association between logFC induced by 2c or 7c cocktails and signatures of aging and OSKM reprogramming was examined with GSEA-based methods using top 500 statistically significant genes (adjusted p-value < 0.05) with the highest absolute logFC from the corresponding signature. Pairwise Spearman correlation for gene expression and protein abundance changes induced by chemical reprogramming as well as transcriptomic signatures of aging and OSKM reprogramming was calculated based on the union of top 650 genes with the lowest p-value for each pair of signatures.

For the identification of enriched functions affected by 2c or 7c treatment, we performed functional GSEA[44] on a pre-ranked list of genes or proteins based on $\log_{10}$(p-value) corrected by the sign of regulation, calculated as:

$$-log(pv) \times sgn(lfc),$$

where *pv* and *lfc* are p-value and logFC of a certain gene, respectively, obtained from edgeR output, and *sgn* is the signum function (equal to 1, -1 and 0 if value is positive, negative or equal to 0, respectively). Gene ontology: biological process (GObp), HALLMARK, KEGG and REACTOME ontologies from the Molecular Signature Database (MSigDB) were used as gene sets for GSEA. The GSEA algorithm was performed separately for each cocktail and age group via the *fgsea* package in R with 5000 permutations. p-values were adjusted with Benjamini-Hochberg method. An adjusted p-value cutoff of 0.1 was used to select statistically significant functions. A similar analysis was performed for gene expression signatures of aging and OSKM reprogramming.

Transcriptomic clock analyses

To assess the transcriptomic age (tAge) of fibroblasts treated with chemical reprogramming reagents, we applied multi-tissue mouse transcriptomic clocks based on the identified signatures of aging[43]. Filtered RNAseq count data was passed to log transformation and scaling. The missing values corresponding to clock genes not detected in the data were imputed

with the precalculated average values. Pairwise differences between average tAges of fibroblasts subjected to chemical reprogramming and corresponding controls were assessed using independent t-tests.

Measurement of splicing damage

The RNA sequencing reads were aligned to the mouse genome (mm10) using STAR with the parameters "--chimSegmentMin 2 --outFilterMismatchNmax 3 --alignEndsType EndToEnd", and PSI values were calculated using rMATS[45]. To identify the alternative splicing changes after compounds treatment, we compared the alternative splicing events between 7c treatment and paired control sample, and selected the events with significant differences (with the cutoff of $|\Delta PSIavg| > 0.1$, and FDR < 0.05). To quantify the overall damage caused by splicing changes, we also counted the proportion of the events that may disrupt protein function. In detail, we predicted the functional consequence for each alternative splicing event, and counted the following three categories for each sample: (1) Introduction of a premature stop codon; (2) Production of frameshifted proteins; and (3) Loss of a peptide in a protein domain region.

Sample processing for quantitative TMT-proteomic analysis

For TMT18-plex proteomics, a slightly-modified form of published procedures was utilized[46,47]. In brief, fibroblasts were seeded at a density of 1 million cells per 10 cm dish and were treated with the specified compounds for 6 days (media replaced once after 3 days) at 37°C, 5% CO_2, 3% O_2. Following completion of the incubation period, cells were rinsed twice with cold PBS and scraped and collected in 0.4 ml of modified RIPA buffer (50 mM KPO_4 (pH 7.5), 150 mM NaCl, 1% Triton X-100, 0.5% deoxycholate, 1% SDS, and 1X protease and phosphatase inhibitors). Samples were then vortexed for 30 seconds, placed on ice for 10 minutes, and pelleted at 21,000 x g for 10 minutes (4°C). The supernatants were transferred to fresh microfuge tubes, and protein concentration was measured by BCA assay (ThermoFisher, Waltham, MA). Then, 200 µg of each protein sample was reduced with 5 mM TCEP, alkylated with 10 mM iodoacetamide, quenched with 10 mM DTT, and chloroform-methanol precipitated. The protein pellets were briefly dried in a speed-vac and resuspended in 100 µl of 200 mM EPPS, pH 8.5. Protein samples were digested with 1:100 Lys-C:protein overnight at room temperature, followed by 1:100 trypsin:protein for 6 hours at 37°C.

The samples were then labeled with tandem mass tag (TMTpro) reagents[46]. Acetonitrile was added to a final volume of 30% prior to adding the TMTpro labeling reagent. For protein level analysis, ~50 µg of peptides were labeled with 100 µg of TMT. For phosphopeptide analysis, we

estimated the phosphopeptide enrichment to be ~1.5:100 and so ~30 µg of peptides were labeled with 60 µg of TMT. Labeling occurred at room temperature for 1h. ~2 µg of peptide from each sample was pooled, desalted and analyzed by mass spectrometry to check labeling efficiency.

TMT labeling efficiency was determined using the "label-check" sample, which is a quality control step prior to the final pooling of TMT-labeled samples. Here, we combined a small amount (1-3 µl or ~2µg) of each sample and analyzed it by mass spectrometry to confirm that peptide digestion was successful, if the degree of labeling was sufficient, and if the labeled samples contained approximately equal amount of peptides. During database searching, the TMTpro label was considered a variable modification at the N-terminus and at lysine residues. We then determined the labeling efficiency for the N-terminus and the lysine residues by dividing labeled N-terminal peptides by total peptides and then labeled lysine-containing peptides by the total lysine-containing peptides. The labeling efficiency should be greater than 95% before proceeding with the analysis. Once labeling efficiency was verified (here, >97%), hydroxylamine was added at a final concentration of ~0.3% and incubated for 15 min. at room temperature. The remaining samples were pooled at a 1:1 ratio across all channels.

To enrich phosphopeptides, the pooled sample was desalted over a 200 mg SepPak column and phosphopeptides were enriched with the Pierce High-Select Fe-NTA Phosphopeptide enrichment kit following manufacturer's instructions. The eluate was desalted via StageTip[48] and is ready for MS analysis. The washes and the unbound fraction of this enrichment were desalted and used for proteome-level analysis.

For proteome-level analysis, the pooled sample was fractionated using basic-pH reversed-phase (BPRP) Liquid Chromatography using an Agilent 1200 pump with an Agilent 300Extend C18 column (2.1 mm ID, 3.5 µm particles, and 250 mm in length). The flow rate over the column was 0.25 mL/min and we used 50-min linear gradient with 5% to 35% acetonitrile in 10 mM ammonium bicarbonate pH 8. Ninety-six fractions were collected and concatenated into 24 superfractions prior to desalting[49]. These 24 superfractions were sub-divided into two groups, each consisting of 12 non-adjacent superfractions. These superfractions were subsequently acidified with 1% formic acid and vacuum centrifuged to near dryness. Each superfraction was desalted via StageTip[48]. Once dried by vacuum centrifugation, the sample was reconstituted using 5% formic acid and 5% acetonitrile prior to acquisition of LC-MS/MS data.

Mass spectrometry data collection and processing

Mass spectrometric data were collected on an Orbitrap Fusion Lumos mass spectrometer, both which are coupled to a Proxeon NanoLC-1200 UHPLC and a FAIMSpro interface[50]. The

100 µm capillary column was packed with 35 cm of Accucore 150 resin (2.6 µm, 150 Å; ThermoFisher Scientific).

Data for the protein superfractions were acquired on an Orbitrap Lumos with a CV set of -40/-60/-80V over a 90 min gradient using Realtime search (RTS)-MS3. The scan sequence began with an MS1 spectrum (Orbitrap analysis, resolution 60,000, 350−1350 Th, automatic gain control (AGC) target 5 x10^5, maximum injection time 100 ms). MS2 analysis consisted of collision-induced dissociation (CID), quadrupole ion trap analysis, automatic gain control (AGC) 2 x10^4, NCE (normalized collision energy) 35, q-value 0.25, maximum injection time 120 ms), and isolation window at 0.5 Th. RTS was enabled and quantitative SPS-MS3 scans (resolution of 50,000; AGC target 2.5x10^5; max injection time of 250 ms) with a real-time false discovery rate filter implementing a modified linear discriminant analysis. For FAIMS, the dispersion voltage (DV) was set at 5000V, the compensation voltages (CVs) used were -40V, -60V, and -80V, and the TopSpeed parameter was set at 1 sec.

For phosphopeptide profiling, data were acquired using two injections on an Orbitrap Lumos one with a CV set of -40/-60/-80V and a second injection with a CV set of -30/-40/-50V, both over a 150 min gradient. A 1sec TopSpeed cycle was used for each CV. The scan sequence began with an Orbitrap MS1 spectrum with the following parameters: resolution: 60,000, scan range: 350-1350 Th, automatic gain control (AGC): 100%, and maximum injection time: 118 ms. MS2 analysis consisted of higher-energy collisional dissociation (HCD) with the following parameters: resolution: 50,000, AGC: 300%, normalized collision energy (NCE): 36%, maximum injection time: 250 ms, and isolation window: 0.7 Th, and. In addition, unassigned, singly, and > 5+ charged species were excluded from MS2 analysis and dynamic exclusion was set to 60 s.

Once the spectra were converted to mzXML using MSconvert[51], database searching could be performed. Database searching included all mouse entries from UniProt (downloaded March 2022). which was concatenated with a version of the database in which the order of the amino acid residues of each protein was reversed. Database searches used a 50-ppm precursor ion tolerance and a product ion tolerance of 0.03 Da. We have traditionally used the 50ppm mass tolerance for our Sequest, and now Comet, database searches. These wide mass tolerance windows were chosen to maximize sensitivity in conjunction with Comet searches and linear discriminant analysis[52,53]. For static modifications, lysine residues and peptide N-termini were modified with +304.207 Da due to the TMTpro labels. Meanwhile, all cysteine residues were modified with iodoacetamide (carbamidomethylation) that results in a +57.021 Da increase in mass. Also, methionine oxidation (+15.995 Da) was set as a variable modification. Likewise, deamidation (+0.984 Da) at glutamine and asparagine residues and phosphorylation (+79.966

Da) at serine, threonine, and tyrosine residues were also set as variable modifications for phosphopeptide enrichment. The false discovery rate (FDR) was set at 1% at the peptide level with filtering a linear discriminant analysis[54]. The protein lists were assembled further to a final protein-level FDR of 1%. The intensities of reporter ions were corrected for the isotopic impurities of the different TMT reagents[55]. For each protein, the peptide summed signal-to-noise (S/N) measurements were summed and normalized to account for equal protein loading by equating the sum of the signal for all proteins in each channel.

For further processing, normalized Uniprot ID-level intensities were summed and $\log_2$ transformed to obtain unique intensities at the level of gene symbol identifiers. Differential abundance analysis was performed with msqrob2[56,57] (https://github.com/statOmics/msqrob2), where we included treatment (control, 2c, or 7c), age group (4 months, or 20 months), and the treatment:age group interaction as covariates. For the phosphoproteomics data, the normalized relative phosphopeptide intensities were $\log_2$ transformed. Differential abundance analysis at the level of these normalized relative $\log_2$ phosphopeptides intensities was again performed in msqrob2[56,57] with the same covariates as for the proteomics analysis. We performed GSEA to obtain protein-level enrichments from the phosphopeptides. To obtain pathway enrichments for both the proteomics and phosphoproteomics data, we ran the GSEA algorithm with the HALLMARK, KEGG, and REACTOME ontologies from the Molecular Signature Database[44] (MSigDB). For kinase substrate enrichment analysis, we performed GSEA using the mouse kinase substrate dataset from PhosphoSitePlus[58] (last updated on April 19th, 2023).

Seahorse assays

Fibroblasts treated with vehicle, 2c, or 7c for 6 days as described above were seeded on 24-well cell culture plates overnight at 37°C, 5% CO_2, 3% O_2 at a cell density of 50,000 cells per well. The following morning, the cells were aspirated and the media was replaced with 500 µl of XF DMEM medium (pH 7.4) supplemented with 1 mM sodium pyruvate, 2 mM glutamine, and 10 mM glucose. Cells were incubated for 1 hour at 37°C in a non-CO_2 incubator prior to assessment of oxygen consumption rate (OCR) and extracellular acidification rate (ECAR) on a XeF24 Extracellular Flux Analyzer (Agilent Technologies, Santa Clara, CA) using a standard Mito Stress protocol[59]. Immediately following the end of the run, cells were stained with LCS1 nuclear green and cells were counted on a SpectraMax i3 plate reader (Molecular Devices, San Jose, CA). OCR and ECAR measurements were then normalized to cell count per well.

Preparation of metabolite samples

Cells were incubated with their respective treatments for 6 days, and then the cells were rinsed with ice-cold 0.9% saline solution. After rinsing, cells were scrapped into 1 ml of 0.9% saline solution, spun at 2,000 x g for 2 minutes (4°C), aspirated, and flash frozen in liquid nitrogen. To extract metabolites, the cells were thawed, lysed in 400 µl of ice-cold methanol, 200 µl of ice-cold chloroform was added, and then another 200 µl of chloroform and 300 µl of ultrapure water was added and the resulting mixture was vortexed for 30 seconds. Following incubation on ice for 10 minutes, the samples were spun at 4,000 rpm for 10 minutes (4°C), and the upper polar phases (600 µl) were transferred to fresh microfuge tubes and stored at -80°C until ready for analysis by mass spectrometry. For normalization of metabolite peak area values, 400 µl of methanol was added to the leftover samples (consisting of nonpolar phases and precipitated protein), and the samples were vortexed and spun at 20,000xg for 5 minutes (4°C). Protein pellets were then aspirated, air-dried for 30 minutes, and resuspended in 500 µl of modified RIPA buffer. Protein concentrations were measured by BCA assay (ThermoFisher, Waltham, MA), and metabolite peak areas were divided by the total µg of protein in each sample.

Metabolite profiling

Hydrophobic interaction liquid chromatography (HILIC) positive ionization profiling was carried out on a Shimadzu Nexera X2 U-HPLC (Shimadzu Corp.; Marlborough, MA) coupled to a Exactive Plus hybrid quadrupole Orbitrap mass spectrometer (Thermo Fisher Scientific; Waltham, MA) according to a published procedure[60]. Protein was precipitated from 10 µl of sample by addition of nine volumes of 74.9:24.9:0.2 v/v/v acetonitrile/methanol/formic acid containing internal standards (valine-d8, Sigma-Aldrich; St. Louis, MO; and phenylalanine-d8, Cambridge Isotope Laboratories; Andover, MA). Precipitated material was cleared by centrifugation and the supernatant was injected directly onto a 150 x 2 mm 3 µm Atlantis HILIC column (Waters; Milford, MA). Elution was as follows: (1) 5% mobile phase A (10 mM ammonium formate and 0.1% formic acid in water), 0.5 min, 250 µl/min; (2) linear gradient to 40% mobile phase B (acetonitrile with 0.1% formic acid), 10 min, 250 µl/min. MS analysis was with electrospray ionization (ESI) in positive ion mode with the following parameters: full scan analysis over 70–800 m/z at 70,000 resolution and 3 Hz data acquisition rate; sheath gas 40; sweep gas 2; spray voltage 3.5 kV; capillary temperature 350°C; S-lens RF 40; heater temperature 300°C; microscans 1; automatic gain control target 1e6; and maximum ion time 250 ms.

HILIC negative ionization profiling[60] was carried out on an Shimadzu Nexera X2 U-HPLC (Shimadzu Corp.; Marlborough, MA) coupled to a Q Exactive Plus hybrid quadrupole orbitrapmass spectrometer (Thermo Fisher Scientific; Waltham, MA). Protein was precipitated

from 30 µl of sample by addition of four volumes of 80% methanol containing internal standards (inosine-15N4, thymine-d4 and glycocholate-d4; Cambridge Isotope Laboratories; Andover, MA). Precipitated material was cleared by centrifugation and the supernatant was injected directly onto a 150 x 2.0 mm Luna NH2 column (Phenomenex; Torrance, CA). Elution was as follows: (1) 10% mobile phase A (20 mM ammonium acetate and 20 mM ammonium hydroxide in water) and 90% mobile phase B (10 mM ammonium hydroxide in 75:25 v/v acetonitrile/methanol), 400 µl/min; (2) linear gradient to 100% mobile phase A, 10 min, 400 µl/min. MS analysis was with electrospray ionization (ESI) in the negative ion mode with the following parameters: full scan analysis over m/z 70–750 at 70,000 resolution and 3 Hz data acquisition rate; sheath gas 55; sweep gas 10; spray voltage −3.0 kV; capillary temperature 350°C; S-lens RF 50; heater temperature 325 °C; microscans 1; automatic gain control target 1e6; and maximum ion time 250 ms.

Raw data was processed using TraceFinder (Thermo Fisher Scientific; Waltham, MA) and Progenesis QI (Nonlinear Dynamics; Newcastle upon Tyne, UK) for Q Exactive (Plus) experiments or MultiQuant (SCIEX; Framingham, MA) for 5500 QTRAP experiments. Metabolite identities were confirmed using authentic reference standards or reference samples.

Statistical analyses and rigor

Each independent biological replicate for this study consists of fibroblasts isolated from a single mouse treated with each cocktail. A technical replicate represents fibroblasts from the same mouse with the same treatment, but measured independently. All measurements in this study consist of at least 3 independent biological replicates. The type I error rate was controlled at the 5% level, either by student's t-test, or by controlling the family-wise error rate at 5% by one-way ANOVA and Tukey's post-hoc analysis, where appropriate. For large omics experiments, the false discovery rate was controlled with the Benjamini-Hochberg procedure at the 5% level, unless stated otherwise.

RESULTS

Partial chemical reprogramming increases pluripotency and mitochondrial OXPHOS activity

For this study, we freshly isolated tail and ear fibroblasts from young (4-month-old, or '4 month') and old (20-month-old, or '20 month') male C57BL/6 mice (**Fig. 1A**). We only used fibroblasts that had been passaged ≤ 3 times to ensure that they maintain their physiologically-relevant aged phenotype in cell culture. Indeed, previous studies have shown that the epigenetic age of fibroblasts increases rapidly once they are cultured *in vitro*[61]. For our study, we used two cocktails: 7c (repsox, trans-2-phenylcyclopropylamine, DZNep, TTNPB, CHIR99021, forskolin,

and valproic acid), which can reprogram somatic cells to pluripotency[31,32]; and 2c (repsox, trans-2-phenylcyclopropylamine), which is a subset of 7c that does not negatively affect cell proliferation[33]. First, we initiated treatment for 4 days prior to assessing their effects on pluripotency by staining for alkaline phosphatase (AP) activity[62] (**Fig. 1B**). While neither 7c nor 2c treatment appeared to affect fibroblast morphology, 2c treatment dramatically increased the number of cells positive for AP activity in both young and old fibroblasts, an indication of increased pluripotency. In contrast, 7c treatment had no effect on AP activity.

Next, we assessed the effect of partial chemical reprogramming (6 days treatment with 2c or 7c) on resting mitochondrial membrane potential and mitochondrial mass using TMRM fluorescence. Previous studies have established a decline of mitochondrial membrane potential with age[63], that caloric restriction (a well-characterized longevity intervention) acts by increasing mitochondrial membrane potential[64], and that artificially increasing the mitochondrial membrane potential of *C.* elegans extends their lifespan[65]. Thus, characterizing the effect of partial chemical reprogramming on basal mitochondrial membrane potential may be a reporter of its efficacy. We observed a strong increase in normalized TMRM fluorescence upon 2c and 7c treatment, and this effect was mirrored across young and old fibroblasts (**Fig. 1C**). As a control, we pre-treated fibroblasts with the mitochondrial uncoupler CCCP and observed the expected decrease in TMRM signal relative to fibroblasts treated with vehicle. Thus, we concluded that partial chemical reprogramming strongly impacts mitochondrial bioenergetics during basal conditions.

Given these results, we further wanted to establish the effect of partial chemical reprogramming on mitochondrial function. To this end, we performed Seahorse experiments on fibroblasts treated with 7c and 2c (**Fig. 1D**) using the Mito Stress Test protocol[59]. In order to account for the effects of these cocktails on cell proliferation, we stained and counted the cells with LCS1 immediately after the run finished, and normalized the oxygen consumption rates (OCR) to OCR per 10,000 cells. From the raw traces, we observed similar responses between young and old fibroblasts. While 2c and 7c treatment only had minor effects on basal oxygen consumption rates, 7c dramatically increased both proton leak (mitochondrial oxygen consumption with inhibited ATP synthase minus non-mitochondrial respiration) and spare respiratory capacity (uncoupled minus basal respiration). Furthermore, these results were corroborated by the observed increase in mitochondrial mass and magnitude of the mitochondrial membrane potential in response to 7c treatment. Taken together, we concluded that partial chemical reprogramming, particularly with 7c, strongly increases the activity and/or abundance of mitochondrial oxidative phosphorylation (OXPHOS) complexes.

Partial chemical reprogramming ameliorates aging-related changes in gene expression and reduces splicing damage

To investigate the effects of partial chemical reprogramming on gene expression, and in particular on the expression of mitochondrial OXPHOS genes, we performed bulk RNA-seq (**Fig. 2**) on young and old fibroblasts treated for 6 days with 7c and 2c. By principal component analysis (PCA) (**Fig. 2A**), we observed that fibroblasts treated with 7c are strongly separated from control and 2c treatment by principal component 1, whereas control and 2c treated fibroblasts are separated by principal component 2. Furthermore, RNA-seq samples clustered by age, were separated by principal components 3 and 4 (**Supplementary Fig. 1A**), and demonstrated age-related changes in gene expression (**Supplementary Fig. 1B**). However, the number of differentially expressed genes with 2c and 7c treatment (**Fig. 2B**) far exceeded the number of differentially expressed genes modified by age. Accordingly, changes induced by 2c or 7c were highly correlated across tested age groups (Spearman correlation coefficient > 0.8) (**Supplementary Fig. 1C**). We first quantified the effect of partial chemical reprogramming on the expression of pluripotency markers[66-68] and the transcription factors Klf4 and c-Myc (Myc) (**Fig. 2C**). Bend4, Esrrb, and Klf4 were all upregulated following partial chemical reprogramming, and this occurred irrespective of the age of the fibroblasts. However, 2c treatment also upregulated expression of Myc and Sox2, whereas 7c treatment did not. Furthermore, 7c somewhat paradoxically reduced expression of Nanog and Myc. Thus, 2c treatment appeared to have a more pronounced effect on cellular pluripotency, which was supported by the increase in AP-positive cells following partial chemical reprogramming. Moreover, 7c had differing effects on pluripotency despite 2c being a subset of this cocktail. Thus, short-term partial chemical reprogramming with 7c appeared to show a different mechanism than normal OSKM cellular reprogramming[69], whereas 2c in contrast appeared more similar to OSKM reprogramming.

Since the accumulation of numerous types of cellular damage is thought to be causal to the aging process[70], we next wanted to see if partial chemical reprogramming could reverse the accumulation of damaged splice variants. To this end, we characterized the alternative splicing events as a function of age (**Supplementary Fig. 2A**) and quantified the proportion of splicing events that may affect protein function (**Fig. 2D**). For 7c-treated fibroblasts, we observed a significant lowering of splicing-related protein damage. Furthermore, we noticed a marginally-significant elevation of splicing-related damage with age, whereas the relative proportions of alternative splicing events remained unchanged. To further characterize the effect of 7c treatment on alternative splicing, we assessed the distribution of ΔPSI values of differentially spliced ($|\Delta PSI| > 0.1$ & p-value < 0.05) genes for old (**Supplementary Fig. 2B**) and young (**Supplementary Fig.**

2C) fibroblasts, separated by the type of alternative splicing. While the number of differentially-spliced events with positive and negative ΔPSI values for exon skipping was roughly equivalent, there was an excess of events with negative ΔPSI values for intron retention across both age groups. Thus, 7c treatment appeared to reduce splicing damage by decreasing the number of retained introns with functional consequences.

To further characterize gene expression changes induced by 2c and 7c, we assessed their association with previously established signatures of OSKM reprogramming and aging[26,43]. Consistent with previous results, we observed significant positive association between signatures of OSKM reprogramming, both in mice and humans, and gene expression changes induced by 2c treatment in fibroblasts from both age groups (**Fig. 2E**). In contrast, transcriptomic profiles of fibroblasts treated with 7c didn't exhibit consistent positive association with markers of OSKM-induced iPSCs. Besides, gene expression changes induced by both 2c and 7c were negatively associated with signatures of aging corresponding to different tissues and mammalian species, suggesting that partial chemical reprogramming may indeed counteract molecular features of aging.

Partial chemical reprogramming increases the abundance of mitochondrial OXPHOS complexes

To elucidate the effects of partial chemical reprogramming on cellular function, we performed multi-plexed proteomics (**Fig. 3**) using isobaric tandem mass tags[46]. PCA based on the normalized protein abundances (**Fig. 3A**) showed strong separation of 7c (principal component 1) and 2c (principal component 2) treatments from control. This effect was further visualized by heatmap (**Fig. 3B**), which demonstrated that 7c treatment had a much more profound effect than 2c. Protein abundances and gene expression changes induced by 2c or 7c treatments were well correlated with each other (**Fig. 3C, Supplementary Fig. 3A**), with Spearman correlation coefficients > 0.7. Furthermore, genes differentially expressed at both the mRNA and proteins levels (**Supplementary Fig. 3A**) following partial chemical reprogramming were generally conserved across the age groups and treatments (**Supplementary Fig. 3B**). Finally, by Pearson correlation analyses of proteomics samples (**Supplementary Fig. 3C**), we observed clustering by both treatment type and age group. Thus, we concluded that 7c treatment had a profound effect on the cellular proteome, and that our proteomics and RNA-seq analyses were in general agreement with each other.

To gain insight into the functional processes associated with the observed anti-aging effect of partial chemical reprogramming, we performed gene set enrichment analysis (GSEA) of the gene expression and protein abundance changes produced by 2c and 7c, along with signatures

of aging and OSKM reprogramming (**Fig. 3D**). During aging, we observed a significant upregulation of pathways involved in inflammation, apoptosis, and p53 signaling, accompanied by a downregulation of genes related to energy metabolism and DNA repair. In contrast, OSKM reprogramming in both human and mouse models counteracted most of these changes. Interestingly, treatment with 2c and 7c also produced multiple anti-aging effects, particularly at the protein level, including upregulation of OXPHOS, TCA cycle, fatty acid metabolism, and mitochondrial translation, and downregulation of interferon signaling. Surprisingly, genes and proteins associated with p53 pathway were upregulated by both cocktails. Partial chemical reprogramming also affected the abundance of proteins involved in cellular differentiation and extracellular matrix organization, resembling the effect of OSKM-induced iPSCs. Finally, 7c treatment resulted in a significantly lower concentration of proteins associated with the PI3K/Akt/mTOR signaling, suggesting that this intervention may induce pro-longevity mechanisms, extending both the healthspan and lifespan of an organism. Thus, partial chemical reprogramming ameliorated multiple molecular features of aging at the level of individual genes, proteins and cellular pathways, and reproduced several effects of OSKM reprogramming.

Since the anti-aging effects of partial chemical reprogramming on the proteome were more pronounced than their effects on the transcriptome, we then used GSEA on the proteomics data to find pathways affected by 7c and 2c treatments (**Supplementary Fig. 4A**). Many mitochondrial-related processes were upregulated by partial chemical reprogramming, whereas only functions related to cell proliferation and cell cycle were downregulated. In particular, all mitochondrial OXPHOS complexes (I-V, **Fig. 3E**) were upregulated for both treatments in both age groups. Proteins essential for mRNA splicing were downregulated by both age and partial chemical reprogramming, although 7c downregulated more splicing-involved proteins than 2c (**Supplementary Fig. 4B**). Additionally, proteins essential for RNA methylation were upregulated in both 2c and 7c-treated fibroblasts, with more pronounced effects observed with 7c. This observation could be relevant for the reduced splicing damage after 7c treatment, as RNA methylation is known to affect mRNA splicing[71]. Finally, we studied the effects of partial chemical reprogramming on other proteins relevant for aging, such as chaperones[72], collagens[73], and proteins implicated in the mitochondrial unfolded protein response[74] (UPR^{mt}, **Supplementary Fig. 4B**). Whereas UPR^{mt} was upregulated by both 7c and 2c, chaperones were significantly upregulated only by 7c treatment, and collagen proteins were down in 7c and up in 2c. Taken together, these results suggested that partial chemical reprogramming strongly upregulated mitochondrial function, with 7c treatment having a more profound effect.

Finally, we examined Spearman correlation of changes in both mRNA and protein abundance induced by 2c and 7c with gene expression signatures of OSKM reprogramming and aging (**Fig. 4**). Consistent with our previous findings, we observed a significant positive association between OSKM reprogramming features and the effects of 2c, both at the gene expression and protein abundance levels. Furthermore, the transcriptomic and proteomic changes induced by 2c and 7c were negatively correlated with multiple signatures of mammalian aging. Therefore, partial chemical reprogramming demonstrated the ability to reduce molecular signatures of aging at both the protein and mRNA levels.

Partial chemical reprogramming phosphorylates mitochondrial proteins and activates Prkaca signaling

In addition to using multi-plexed proteomics to quantitatively ascertain overall effects on protein expression, we also evaluated the effects of partial chemical reprogramming on protein phosphorylation and kinase signaling by using TMT-based phosphoproteomics (**Fig. 5**). First, we performed GSEA on the normalized relative phosphopeptide intensities. Across all treatments and age groups, we observed decreased phosphorylation of proteins involved in cell migration and proliferation, and conversely increased phosphorylation of proteins essential to fatty acid metabolism, signaling and transport of ions, and muscle development and contraction (particularly in 2c-treated fibroblasts) (**Supplementary Fig. 5**). More generally, shared across 2c and 7c treatments was an upregulation in the phosphorylation of mitochondrial proteins (**Fig. 5A**). In addition, for 2c-treated fibroblasts, proteins involved in lipolysis and constructing muscle were also increasingly phosphorylated. Although 7c treatment reduced splicing damage (**Fig. 2E**), we observed no statistically-significant changes in the phosphorylation of proteins required for mRNA splicing. Overall, we determined that 2c and 7c treatment share a common mechanism in upregulating OXPHOS activity by phosphorylating mitochondrial proteins, with 7c having a stronger effect relative to 2c. We also observed that 2c treatment activated additional pathways (lipolysis and muscle contraction) compared to 7c.

To dive deeper into the mechanisms of partial chemical reprogramming, we analyzed kinase signaling pathways affected by 2c and 7c treatments (**Fig. 5B**). For all treatments and age-groups, only Prkaca signaling was significantly (FDR < 0.05) and consistently upregulated. Notably, Prkaca, the catalytic alpha subunit of the cAMP-activated protein kinase A, is crucial for regulating glucose metabolism, and upon activation, for increasing lipolysis and energy expenditure in white adipose tissue[75]. Thus, it is interesting that this kinase was activated by 7c treatment when no statistically-significant effect on lipolysis was observed with this treatment. In

contrast, in young fibroblasts, Akt1 and Mapk1 signaling was significantly upregulated and downregulated, respectively upon 2c treatment. Both pathways were also strongly affected by 2c treatment in old fibroblasts, but did not reach statistical significance (FDR < 0.05). Mapk1 and Akt1 have opposing effects on regulating the expression of structural constituents of muscle[76]; thus, this observed influence is entirely consistent with upregulation of proteins involved in muscle contraction by 2c treatment. Therefore, we concluded that 2c and 7c share similar mechanisms of partial chemical reprogramming via activation of Prkaca signaling and mitochondrial phosphorylation. However, activation of Prkaca by 7c treatment had different downstream effects than by 2c treatment.

Partial chemical reprogramming reverses the accumulation of aging-related metabolites

As the levels of endogenous cellular metabolites can have both activating and inhibitory effects on various signaling pathways, we performed an untargeted mass spectrometry-based analysis of metabolites following partial chemical reprogramming (**Fig. 6**). We analyzed the abundance of polar metabolites (polar fraction taken from chloroform-methanol extraction of cell pellets) by hydrophobic interaction liquid chromatography (HILIC)[77,78]. Again, to account for the effects of chemical reprogramming cocktails on cell proliferation rates, we measured the protein concentration in each cell pellet by BCA assay, and normalized the peak area of each metabolite by the µg of protein per sample. By PCA analysis (**Supplementary Fig. 6A**), we saw a clear separation of 7c treatment from control and 2c by principal component 1, whereas only young fibroblasts treated with 2c were separated from control by principal component 2. As expected, Pearson correlations between samples (**Supplementary Fig. 6B**) were high (> 0.9), and they were separated based on their respective treatments by hierarchical clustering (**Fig. 6A**). In total, of 203 metabolites detected, 109 were significantly altered by partial reprogramming treatment (**Fig. 6B**) when tested by one-way ANOVA.

We visualized the metabolites altered by partial chemical reprogramming by heatmap (**Fig. 6C**), which confirmed that 7c treatment had a much more pronounced effect on the metabolome than 2c, in agreement with the gene expression and proteomics data. Analysis of the top 50 significantly altered metabolites (**Fig. 6D**) revealed a cluster of 6 metabolites strongly upregulated by 7c treatment (guanidoacetic acid, S-adenosylhomocysteine (SAH), tyramine, tributylamine, trimethylamine N-oxide, and atenolol). Interestingly, SAH is known as an inhibitor of DNA methyltransferases, both by product build-up and by competitive inhibition[79,80]. Thus, the increased abundance of SAH upon 7c treatment could stem from changes in epigenetic regulation through the activity of DNA methyltransferases, especially since protein levels of Mat2a were

decreased by 7c treatment (**Fig. 6E**, top). Guanidoacetic acid, on the other hand, is the biosynthetic precursor of creatine and accepts a donor methyl group from S-adenosyl methionine[81] (SAM). Therefore, the effects of 7c treatment on guanidoacetic acid and SAH levels were intertwined. Conversely, many metabolites were strongly downregulated by 7c treatment, including 3',5' cyclic AMP (an activator of protein kinase A[75]), xanthine (an inhibitor of phosphodiesterases that increase cyclic AMP levels[82]), and various other purines, nucleosides, and nucleotides (hypoxanthine, inosine, pseudouridine, uridine, uracil, adenosine, and guanosine). In agreement with this observation, proteins involved in xanthine metabolism (**Fig. 6E**, bottom) were upregulated by partial chemical reprogramming with 7c. Moreover, several purine degradation metabolites have been shown to be positively associated with aging[83], suggesting that 7c treatment may reverse the accumulation of aging-related metabolites.

In the case of 2c treatment, two upregulated and related metabolites stood out: serotonin, and its biosynthetic precursor 5-hydroxy-tryptophan (5-HTP), which is decarboxylated to form serotonin[84]. Besides being an important neurotransmitter, serotonin and its precursor 5-HTP are formed downstream from tryptophan by tryptophan hydroxylase and 5-HTP decarboxylase.[84] While the abundance of tryptophan itself was not altered by partial reprogramming, the abundance of niacinamide, which is also synthesized from tryptophan[85], was slightly reduced following 2c treatment. Lastly, for 2c, two byproducts of lysine metabolism (Glu-Lys and aminoadipic acid) were downregulated, whereas lysine levels were not statistically altered. Since lysine is crucial for the cross-linking of collagen fibrils[86], and since 2c strongly upregulated the expression of collagen proteins (**Fig. 3E**), 2c treatment could be downregulating lysine catabolism. Therefore, we observed strong effects of partial reprogramming on the cellular metabolome, and these effects were generally consistent with the analyses of protein and gene expression. Additionally, partial chemical reprogramming with 7c appeared to reduce the levels of several purine derivatives, which could be important for reducing aging-related accumulation of damaging metabolites.

Partial chemical reprogramming rejuvenates both young and aged cells

To assess the rejuvenation potential of partial chemical reprogramming, we analyzed the effect of 7c and 2c treatment on fibroblast age (**Fig. 7**) using mouse transcriptomic clocks (**Fig. 7A**). As tools to measure age, transcriptomic clocks have successfully reported the effects of interventions known to affect lifespan and rate of biological aging, and appear to be sensitive to transient changes in gene expression that may occur upon short-term treatment with drugs[9,10] and OSKM reprogramming[26]. Application of transcriptomic clocks developed in our lab to the bulk

RNA-seq dataset (presented in **Fig. 2**) revealed a significant lowering of both chronological and biological age with short-term 7c treatment; however, there appeared to be only a minor effect on of biological tAge in young fibroblasts treated with 2c. We also measured DNA methylation (DNAm) by microarrays following partial chemical reprogramming, and analyzed the results using relevant epigenetic clocks[87] (**Fig. 7B**). As a positive control, we also measured the epigenetic age (DNAmAge) of young and old fibroblasts reprogrammed by OSKM expression (**Supplementary Fig. 7**). We found a consistent lowering of DNAmAge in response to 7c treatment, whereas the effect of 2c treatment was weaker and more variable, depending on the clock used. As expected, fibroblasts isolated from old mice were epigenetically older than fibroblasts taken from young mice, which further confirmed that the fibroblasts maintained their aged phenotype in cell culture. Finally, fully-reprogrammed fibroblasts (iPSCs) demonstrated an epigenetic age of approximately 0, which was consistent with previous reports[8]. Therefore, we concluded that partial chemical reprogramming, particularly by 7c treatment, can rejuvenate both young and aged cells.

DISCUSSION

The goal of our study was to characterize the effects of partial chemical reprogramming of cells at the level of the epigenome, transcriptome, proteome and phosphoproteome, and metabolome. To do this, we used low-passage fibroblasts isolated from young (4-month-old) and old (20-month-old) C57BL/6 male mice and treated the fibroblasts with two chemical reprogramming cocktails (2c and 7c). We then analyzed the effects of partial chemical reprogramming and its relationship to aging using a suite of omics-based approaches. Finally, we combined these multi-omics assays with measures of biological age (by using aging clocks) and cellular function (by utilizing respirometry and fluorescence microscopy to determine the effects of partial chemical reprogramming on mitochondrial bioenergetics). Together, these studies evaluated the potential for partial chemical reprogramming to ameliorate aging features, and uncovered its associated mechanisms for further optimization and development of treatments that could slow and/or reverse aging *in vivo*.

Based on measurements of biological age using epigenetic and transcriptomic clocks, we concluded that partial chemical reprogramming with 7c is able to rejuvenate fibroblasts taken from both young and old mice. Additionally, from measures of mRNA, protein, and phosphoprotein abundances, we determined that partial chemical reprogramming causes wide scale changes to fibroblast gene expression that are larger in magnitude than the changes that occur due to aging. Based on GSEA analyses of these multi-omics data, we uncovered that the most prominent mechanistic signature of partial chemical reprogramming is the upregulation of mitochondrial

oxidative phosphorylation, which further manifested as a functional increase in spare respiratory capacity and increased mitochondrial transmembrane potential. Notably, the data suggested that the activation of the cAMP-dependent protein kinase A by partial chemical reprogramming may be crucial for mediating the upregulation of mitochondrial OXPHOS. Finally, we showed that partial chemical reprogramming can reverse molecular damage positively associated with aging, including the accumulation of aging-related metabolites and mispliced mRNA.

The downregulation of mitochondrial OXPHOS and translation is a known signature of aging[42,43]; furthermore, several recent studies have highlighted that augmenting the mitochondrial transmembrane potential can increase longevity[64,65]. In this light, we suggest that partial chemical reprogramming of fibroblasts induces rejuvenation, at least in part, by upregulating mitochondrial OXPHOS. Importantly, this differs significantly from OSKM reprogramming, which shows a strong glycolytic shift in response to the induction of OSKM expression[88]. Furthermore, our results are consistent with the activation of different transcription factors by partial chemical reprogramming with 7c, which showed negligible expression of the Yamanaka factors, increased expression of two pluripotency markers (Esrrb and Bend4), and decreased expression of Nanog.

The results of several recent studies have illustrated the changes in mitochondrial ultrastructure that occur during aging[89-91], which may result from several interdependent mechanisms such as disrupted OPA1-,Drp1-, and MICOS-mediated fission and fusion dynamics[92-96], decreased cardiolipin content[97], destabilized ATP synthase dimers[98], and uncontrolled opening of the mitochondrial permeability transition pore[99,100]. Importantly, mitochondrial ultrastructure determines bioenergetic function and thus, detrimental changes to mitochondrial ultrastructure (such as loss of tight cristae junctions and cristae curvature) can lead to bioenergetic declines during aging[101,102]. These declines include increased proton leak and reactive oxygen species production[101-103], decreased respiratory supercomplex assembly and associated spare respiratory capacity[102,104], and impaired proteostasis[105,106]. Thus, the activation of factors that reinforce proper mitochondrial ultrastructure could reverse many aging-related elements of mitochondrial dysfunction.

Downstream from the activation of distinct transcription factors by partial chemical reprogramming is the activation (by phosphorylation of the catalytic subunit alpha) of protein kinase A, which functions as a master regulator of energy storage, metabolism, and G-protein-coupled-receptors[107,108]. In fact, protein kinase A can become anchored to both the inner and outer mitochondrial membranes, where it goes on to phosphorylate mitochondrial proteins such as Complex I (to upregulate OXPHOS), Drp1 (to regulate mitochondrial fission and fusion dynamics), and the pro-apoptotic protein BAD (to increase cell survival)[109,110]. This tethering of

protein kinase A to mitochondrial membranes is dependent on the activity of several A-kinase anchoring proteins, which additionally can recruit phosphatases to counteract excessive protein kinase A activity[109,110]. Thus, the upregulation of OXPHOS by partial chemical reprogramming may primarily stem from the sustained activation of protein kinase A and its subsequent localization to mitochondria. Moreover, the rejuvenating effects of partial chemical reprogramming via protein kinase A activation are further validated by studies showing that knock-out of the regulatory subunit RIIβ extends mouse lifespan and ameliorates aging-related declines in health[111].

In conclusion, we have shown that partial chemical reprogramming is able to reverse many signs of aging in a mouse fibroblast model. We thus posit that partial reprogramming by chemicals may represent a viable alternative to the cyclically-induced, ectopic expression of Yamanaka factors for rejuvenating aged cells. Further testing however, particularly in animal models of aging, is needed to fully elucidate the effectiveness of partial chemical reprogramming *in vivo*, and to establish what advantages, if any, it may have over OSK/OSKM partial reprogramming. In addition, a more thorough characterization of the effect of partial chemical reprogramming on mitochondrial dynamics and function, such as OXPHOS supercomplex assembly, cristae ultrastructure, and protein import, could shed greater light on the importance of various mitochondrial processes in the aging process. Finally, elucidating the molecular targets of chemical reprogramming compounds, whether they may be transcription factors, regulators of the epigenome, and/or various kinases and cellular receptors, could further contribute to our understanding of aging and how to best reverse it.

ACKNOWLEDGEMENTS

The authors would like to thank Dr. William Oldham for assistance with Seahorse measurements, Bobby Brooke for coordinating measurements of DNAm by microarray, Jesse Poganik for assistance with analysis of metabolomics data, and members of the Gladyshev lab for helpful discussions.

The project described was supported by the National Institute of Biomedical Imaging and Bioengineering, National Institutes of Health through grant number T32 EB016652 to W.M, by NIA grants to V.N.G., and by NIH/NIGMS grant R01 GM132129 (to J.A.P.) and GM67945 (to S.P.G.).

CONTRIBUTIONS

W.M designed the study, conducted the experiments, and wrote the original draft. L.J.E.G analyzed proteomics data. A.T performed GSEA, and transcriptomic clock and signature analyses. S.Z performed splicing analyses of RNA-seq data. J.A.P performed TMT labeling and acquired mass spectrometry data. K.A.P and A.H.C analyzed the metabolomics samples. C.B.C supervised acquisition of metabolomics data and provided funding. S.P.G supervised acquisition of proteomics data and provided funding. V.N.G designed and supervised the study and provided funding. All authors contributed to the revision of the manuscript.

FIGURE LEGENDS

Figure 1: Functional effects of partial chemical reprogramming

A. Overview of the study. Tail and ear fibroblasts were isolated from young (4-month-old) and old (20-month-old) male C57BL/6 mice, and cryo-stocks were prepared once reaching ~80-90% confluency (passage number P1). All fibroblasts used in this study were ≤ P3. These cells were subjected to partial chemical reprogramming followed by indicated analyses. *B. AP staining.* Young and old fibroblasts were treated with 2c, 7c, or DMSO for 4 days, followed by visualization of cells positive for alkaline phosphatase activity with the StemAb™ Alkaline Phosphatase Staining Kit II (4X objective). Scale bars: 126.2 μm (100 pixels). *C. TMRM staining.* Following treatment for 6 days with 2c, 7c, or DMSO, fibroblasts were stained with 250 nM TMRM and 10 μg/ml Hoescht 33342 for 20 minutes at 37°C, 5% CO_2, and 3% O_2. TMRM fluorescence intensity was normalized to the number of nuclei per field, and quantified across 4-5 images from random fields for each independent biological replicate (n = 3). For CCCP treatment, cells were treated with 50 μM CCCP in DMSO for 15 minutes prior to TMRM staining. Error bars represent means ± standard deviations, and data were quantified based on percent change from control-treated fibroblasts. Scale bars: 31.1 μm (100 pixels). Statistical significance was determined by one-way ANOVA and Tukey's post-hoc analysis. *p < 0.05, **p < 0.01, ***p < 0.001. *D. Effects on oxygen consumption.* Top: representative raw traces of oxygen consumption of cells subjected to the Mito Stress Test protocol (basal, followed by 1 μM oligomycin a, 5 μM FCCP, and 1 μM rotenone / antimycin a) following 6 days of partial chemical reprogramming. Error bars represent means ± standard deviations from 3 technical replicates per treatment. Bottom: quantified oxygen consumption rates across 4 independent biological replicates (n = 4, error bars represent means ± standard deviations). Statistical significance was determined by one-way ANOVA and Tukey's post-hoc analysis. *p < 0.05, **p < 0.01, ***p < 0.001.

Figure 2: Effect of partial chemical reprogramming on gene expression

A. PCA analysis of bulk RNA-seq samples. Fibroblasts were treated with 2c, 7c, or control for 6 days followed by RNA-seq analyses. *B. Differentially expressed genes.* Differentially expressed genes were determined using *edgeR* and considered statistically significant at a Benjamini-Hochberg false discovery rate (FDR) cut-off < 0.05. *C. Expression of pluripotency markers.* Effect of partial chemical reprogramming on the normalized expression of pluripotency markers and Klf4 and c-Myc (Myc). Statistical significance was determined with *edgeR*. *p.adjusted < 0.05, **p.adjusted < 0.01, ***p.adjusted < 0.001. *D) Splicing damage.* Splicing damage was determined by the proportion of alternative-splicing events that may disrupt protein function. Statistical significance was determined by one-way ANOVA and Tukey's post-hoc analysis. ^p < 0.1, *p < 0.05. *E. Association of gene expression changes induced by chemical reprogramming with signatures of aging and OSKM reprogramming.* Signatures of aging are labelled in red, whereas signatures of OSKM reprogramming are labelled in cyan. NES: normalized enrichment score. Statistical significance was determined using GSEA. *p < 0.05, **p < 0.01, ***p < 0.001.

Figure 3: Effect of partial chemical reprogramming on protein expression

A. PCA analysis of log_2 normalized protein abundances. Fibroblasts were treated for 6 days with 2c, 7c, or control followed by mass spectrometry-based proteomic analyses. *B. Global effects of partial chemical reprogramming on the proteome.* Scaled heatmap of normalized protein abundances with clustering. *C. Comparisons between effects on protein and gene expression.* Log_2 fold changes of protein (vertical axis) versus mRNA (horizontal axis) for 20-month-old fibroblasts treated with 7c. Spearman correlation coefficient is shown in bold. Labeled are the genes that are most strongly differentially expressed after 7c treatment (adjusted p-value < 0.05) at both the mRNA and protein levels (shown in green). Also depicted are genes significantly changing only at the protein level (shown in cyan), or at the mRNA level (shown in red). Spearman correlation coefficients between protein and mRNA levels were > 0.7 for all treatment conditions (refer to **Supplementary Fig. 3A**). *D. Functional GSEA.* Associations of partial chemical reprogramming (blue: 7c, green: 2c) with signatures of OSKM reprogramming (cyan) and aging (red) at the level of enriched pathways. ^Benjamini-Hochberg p.adjusted < 0.1, *p.adjusted < 0.05, **p.adjusted < 0.01, ***p.adjusted < 0.001. *E. Effect of partial chemical reprogramming on the expression of protein complexes associated with aging.* Protein abundances of mitochondrial OXPHOS complexes, chaperones, collagens, and the spliceosome are all affected by partial chemical reprogramming. Each datapoint represents the abundance of an individual protein. Significance was assessed with a linear regression model that included effects for gene, treatment, age group, and a treatment:age group interaction. p-values within each panel were

corrected for multiple testing with the default Dunnett correction ("single-step") method in the *multcomp* R package[112]. 'Benjamini-Hochberg FDR < 0.1, *FDR < 0.05, **FDR < 0.01, ***FDR < 0.001, n.s. p ≥ 0.1.

Figure 4: Correlation of gene and protein expression changes with signatures of aging and OSKM reprogramming

Spearman correlation of gene expression and protein abundance changes induced by partial chemical reprogramming (blue: 7c, green: 2c) with the signatures of OSKM reprogramming (cyan) and aging (red). Correlation coefficients ρ were calculated by the Spearman method based on the union of top 650 genes with the lowest p-value for each pair of signatures. Statistically significant pairwise correlations with Spearman ρ > 0.1 are labelled with asterisks. ***p.adjusted < 0.001.

Figure 5: Effect of partial chemical reprogramming on the phosphoproteome

A. Targeted GSEA analysis of phosphorylation targets for four selected gene ontologies following partial chemical reprogramming. Bar lengths depict normalized enrichment scores. **Benjamini-Hochberg FDR < 0.01, ***FDR < 0.001. *B. Kinase signaling pathways.* z-values for a kinase enrichment analysis are shown for the effects of partial reprogramming with 2c (horizontal axis) vs. 7c (vertical axis) in young (top) and old (bottom) fibroblasts. Signaling pathways significantly affected (Benjamini-Hochberg FDR < 0.05) by both 7c and 2c treatment (Prkaca) are colored in red, and signaling pathways affected only by 2c in young fibroblasts (Makp1 and Akt1) are colored in green (highlighted in bold for old fibroblasts). Horizontal and vertical red lines indicate the 0.05 Benjamini-Hochberg FDR significance threshold cut-offs for the comparisons 2c vs. control and 7c vs. control, respectively.

Figure 6: Effect of partial chemical reprogramming on the metabolome

A. Hierarchical clustering of polar metabolite samples. Fibroblasts were treated for 6 days with 2c, 7c, or control followed by cell scraping and collection in cold 0.9% saline solution (n = 3 independent biological replicates). Polar metabolites were isolated from the frozen cell pellets by chloroform-methanol extraction, and the upper polar phase was analyzed by hydrophobic interaction liquid chromatography (HILIC) coupled to a quadrupole mass spectrometer in both positive and negative ionization modes[77,78]. All subsequent analyses were performed using MetaboAnalyst 5.0[113]. *B. Metabolites affected by partial chemical reprogramming.* A total of 203 metabolites were identified by HILIC-positive and -negative methods, combined. Metabolite peak

areas were normalized to the µg of protein in each cell pellet (determined by BCA assay) and log-transformed. In total, abundances of 109 metabolites were significantly altered by partial chemical reprogramming (one-way ANOVA $p < 0.05$, colored in red). *C. Global effects of partial chemical reprogramming on the metabolome.* Scaled heatmap of normalized, log-transformed metabolite abundances. *D. Abundances of top 50 metabolites significantly altered by partial chemical reprogramming with 2c or 7c.* Scaled heatmap with labeled metabolites. *E. Expression of metabolite-related proteins.* Expression of proteins related to s-adenosylhomocysteine biosynthesis (top) and xanthine metabolism (bottom) following partial chemical reprogramming with 2c and 7c vs. control in young and old cells. 'Benjamini-Hochberg FDR < 0.1, *FDR < 0.05, **FDR < 0.01, ***FDR < 0.001.

Figure 7: Effect of partial chemical reprogramming on biological age

A. Effect of partial chemical reprogramming on transcriptomic age (tAge). tAge was assessed by using mouse multi-tissue transcriptomic clocks to analyze the bulk RNA-seq data presented in Figure 2 (n = 4 independent biological replicates). *p < 0.05, **p < 0.01, ***p < 0.001. *B. Effect of partial chemical reprogramming on epigenetic age (DNAmAge).* Levels of mean DNA methylation (DNAm) was assessed by DNAm microarray on the Horvath mammal 320k chip (n = 5 independent biological replicates). *p < 0.05, **p < 0.01, ***p < 0.001.

Supplementary Figure 1: Effect of fibroblast age on gene expression changes

A. PCA analysis of bulk RNA-seq samples. Principal components 3 and 4 are shown to highlight effects of age (4-month-old vs. 20-month-old) on fibroblast gene expression *in vitro*. *B. Age-related differentially expressed genes.* Volcano plot (left) of age-related differentially expressed genes (genes with FDR < 0.05 colored in red, differential expression analysis performed using *edgeR*). Gene ontology (GO) enrichment analyses (right) of age-related differentially expressed (FDR < 0.05) genes. Activated genes are genes that are upregulated in old fibroblasts when compared to young; suppressed genes are downregulated in old fibroblasts compared to young. *C. Correlation between gene expression changes induced by chemical reprogramming in young and old fibroblasts.* Spearman correlation coefficients are shown in bold. Labeled are the genes that are most strongly differentially expressed after 2c and 7c treatment (adjusted p-value < 0.05) in young and old fibroblasts (shown in green). Also depicted are genes significantly changing only in old fibroblasts (shown in cyan), or only in young fibroblasts (shown in red).

Supplementary Figure 2: Characterization of alternative splicing events

A. Observed alternative splicing events. Observed alternative splicing events in control samples (n = 4 independent biological replicates) grouped by different types of alternative splicing (A3SS = alternative 3' splice site, A5SS = alternative 5' splice site, IR = intron retention, ES = exon skipping) and age. *B. Distribution of alternative splicing changes in old fibroblasts after 7c treatment.* Each datapoint represents one splicing event that was differentially spliced (|ΔPSI| > 0.1 & p-value < 0.05) following 7c treatment. *C. Distribution of alternative splicing changes in young fibroblasts after 7c treatment.* Each datapoint represents one splicing event that was differentially spliced (|ΔPSI| > 0.1 & p-value < 0.05) following 7c treatment.

Supplementary Figure 3: Additional correlation analyses

A. Comparisons between protein differential abundance and differential gene expression. Shown here for all treatment conditions (top: 2c vs. control, bottom: 7c vs. control. Left panels: young fibroblasts, right panels: old fibroblasts). Spearman correlation coefficients are shown in bold. *B. Correlations between protein and mRNA levels.* Heatmap of Spearman correlation coefficients across all treatment conditions calculated based on the union of top 1000 genes with the lowest p-value for each pair of signatures (blue: 7c, green: 2c). *C. Correlation between log_2 normalized abundances of the proteomics samples.* Heatmap of Pearson correlation coefficients.

Supplementary Figure 4: GSEA of protein abundances

A. GSEA (GObp, HALLMARK, KEGG, and REACTOME) most significantly altered by partial chemical reprogramming. Shown are the top 25 most significant ontologies in each comparison (2c and 7c vs. controls, in young and old fibroblasts). 'Benjamini-Hochberg FDR < 0.1, *FDR < 0.05, **FDR < 0.01, ***FDR < 0.001. *B. Protein abundances of processes affected by partial chemical reprogramming.* Log_2 fold changes of proteins involved in alternative mRNA splicing (left), mitochondrial unfolded protein response (UPR^{mt}, center), and RNA methylation (right). 'Benjamini-Hochberg FDR < 0.1, *FDR < 0.05, **FDR < 0.01, ***FDR < 0.001.

Supplementary Figure 5: GSEA of phosphopeptide abundances

GSEA of phosphorylated pathways significantly altered by partial chemical reprogramming. We show all ontologies with Benjamini-Hochberg FDR < 0.05 in at least one comparison (2c and 7c vs. controls, in young and old fibroblasts). 'Benjamini-Hochberg FDR < 0.1, *FDR < 0.05, **FDR < 0.01.

Supplementary Figure 6: Quality control of metabolite samples

A. PCA analysis of metabolite samples. PCA analysis was performed following normalization and log-transformation of metabolite peak areas. *B. Metabolites samples correlation.* Correlation coefficients r were determined by Pearson method.

Supplementary Figure 7: Expression of pluripotency markers following OSKM reprogramming of fibroblasts

Following doxycycline-induced expression of OSKM in young and old fibroblasts, fully-reprogrammed iPSC colonies were stained for pluripotency markers Sox2 (top), Oct4 (middle), and Nanog (bottom). Representative images obtained from reprogrammed old fibroblasts (left: Hoescht 33342, middle: pluripotency markers, right: merged images). Scale bars: 126.2 µm (100 pixels).

REFERENCES

1 Schumacher, B., Pothof, J., Vijg, J. & Hoeijmakers, J. H. J. The central role of DNA damage in the ageing process. *Nature* **592**, 695-703 (2021). https://doi.org:10.1038/s41586-021-03307-7

2 Hipp, M. S., Kasturi, P. & Hartl, F. U. The proteostasis network and its decline in ageing. *Nature Reviews Molecular Cell Biology* **20**, 421-435 (2019). https://doi.org:10.1038/s41580-019-0101-y

3 Ferrucci, L. & Fabbri, E. Inflammageing: chronic inflammation in ageing, cardiovascular disease, and frailty. *Nature Reviews Cardiology* **15**, 505-522 (2018). https://doi.org:10.1038/s41569-018-0064-2

4 Amorim, J. A. *et al.* Mitochondrial and metabolic dysfunction in ageing and age-related diseases. *Nature Reviews Endocrinology* **18**, 243-258 (2022). https://doi.org:10.1038/s41574-021-00626-7

5 Kane, A. E. & Sinclair, D. A. Epigenetic changes during aging and their reprogramming potential. *Crit Rev Biochem Mol Biol* **54**, 61-83 (2019). https://doi.org:10.1080/10409238.2019.1570075

6 Gems, D. & de Magalhães, J. P. The hoverfly and the wasp: A critique of the hallmarks of aging as a paradigm. *Ageing Res Rev* **70**, 101407 (2021). https://doi.org:10.1016/j.arr.2021.101407

7 Keshavarz, M., Xie, K., Schaaf, K., Bano, D. & Ehninger, D. Targeting the "hallmarks of aging" to slow aging and treat age-related disease: fact or fiction? *Molecular Psychiatry* **28**, 242-255 (2023). https://doi.org:10.1038/s41380-022-01680-x

8 Horvath, S. DNA methylation age of human tissues and cell types. *Genome Biology* **14**, 3156 (2013). https://doi.org:10.1186/gb-2013-14-10-r115

9 Choukrallah, M.-A., Hoeng, J., Peitsch, M. C. & Martin, F. Lung transcriptomic clock predicts premature aging in cigarette smoke-exposed mice. *BMC Genomics* **21**, 291 (2020). https://doi.org:10.1186/s12864-020-6712-z

10 Buckley, M. T. *et al.* Cell-type-specific aging clocks to quantify aging and rejuvenation in neurogenic regions of the brain. *Nature Aging* **3**, 121-137 (2023). https://doi.org:10.1038/s43587-022-00335-4

11 Vaiserman, A. & Krasnienkov, D. Telomere Length as a Marker of Biological Age: State-of-the-Art, Open Issues, and Future Perspectives. *Frontiers in Genetics* **11** (2021). https://doi.org:10.3389/fgene.2020.630186

12 Jansen, R. *et al.* An integrative study of five biological clocks in somatic and mental health. *eLife* **10**, e59479 (2021). https://doi.org:10.7554/eLife.59479

13 Pearce, E. E. *et al.* Telomere length and epigenetic clocks as markers of cellular aging: a comparative study. *Geroscience* **44**, 1861-1869 (2022). https://doi.org:10.1007/s11357-022-00586-4

14 Johnson, A. A., Shokhirev, M. N., Wyss-Coray, T. & Lehallier, B. Systematic review and analysis of human proteomics aging studies unveils a novel proteomic aging clock and identifies key processes that change with age. *Ageing Res Rev* **60**, 101070 (2020). https://doi.org:10.1016/j.arr.2020.101070

15 Krištić, J. *et al.* Glycans are a novel biomarker of chronological and biological ages. *J Gerontol A Biol Sci Med Sci* **69**, 779-789 (2014). https://doi.org:10.1093/gerona/glt190

16 Lu, A. T. *et al.* DNA methylation GrimAge strongly predicts lifespan and healthspan. *Aging (Albany NY)* **11**, 303-327 (2019). https://doi.org:10.18632/aging.101684

17 Sharp, Z. D. & Strong, R. Rapamycin, the only drug that has been consistently demonstrated to increase mammalian longevity. An update. *Experimental Gerontology* **176**, 112166 (2023). https://doi.org:https://doi.org/10.1016/j.exger.2023.112166

18 Shindyapina, A. V. *et al.* Rapamycin treatment during development extends life span and health span of male mice and Daphnia magna. *Science Advances* **8**, eabo5482 (2022). https://doi.org:doi:10.1126/sciadv.abo5482

19 Juricic, P. *et al.* Long-lasting geroprotection from brief rapamycin treatment in early adulthood by persistently increased intestinal autophagy. *Nature Aging* **2**, 824-836 (2022). https://doi.org:10.1038/s43587-022-00278-w

20 Kulkarni, A. S., Gubbi, S. & Barzilai, N. Benefits of Metformin in Attenuating the Hallmarks of Aging. *Cell Metabolism* **32**, 15-30 (2020). https://doi.org:https://doi.org/10.1016/j.cmet.2020.04.001

21 Petkovich, D. A. *et al.* Using DNA Methylation Profiling to Evaluate Biological Age and Longevity Interventions. *Cell Metab* **25**, 954-960.e956 (2017). https://doi.org:10.1016/j.cmet.2017.03.016

22 Zhang, B. *et al.* Multi-omic rejuvenation and lifespan extension upon exposure to youthful circulation. *bioRxiv*, 2021.2011.2011.468258 (2021). https://doi.org:10.1101/2021.11.11.468258

23 Ma, S. *et al.* Heterochronic parabiosis induces stem cell revitalization and systemic rejuvenation across aged tissues. *Cell Stem Cell* **29**, 990-1005.e1010 (2022). https://doi.org:10.1016/j.stem.2022.04.017

24 Yang, J. H. *et al.* Loss of epigenetic information as a cause of mammalian aging. *Cell* **186**, 305-326.e327 (2023). https://doi.org:10.1016/j.cell.2022.12.027

25 Lu, Y. *et al.* Reprogramming to recover youthful epigenetic information and restore vision. *Nature* **588**, 124-129 (2020). https://doi.org:10.1038/s41586-020-2975-4

26 Kriukov, D., Khrameeva, E. E., Gladyshev, V. N., Dmitriev, S. E. & Tyshkovskiy, A. Longevity and rejuvenation effects of cell reprogramming are decoupled from loss of somatic identity. *bioRxiv*, 2022.2012.2012.520058 (2022). https://doi.org:10.1101/2022.12.12.520058

27 Kerepesi, C., Zhang, B., Lee, S. G., Trapp, A. & Gladyshev, V. N. Epigenetic clocks reveal a rejuvenation event during embryogenesis followed by aging. *Sci Adv* **7** (2021). https://doi.org:10.1126/sciadv.abg6082

28 Gladyshev, V. N. The Ground Zero of Organismal Life and Aging. *Trends Mol Med* **27**, 11-19 (2021). https://doi.org:10.1016/j.molmed.2020.08.012

29 Ocampo, A. *et al.* In Vivo Amelioration of Age-Associated Hallmarks by Partial Reprogramming. *Cell* **167**, 1719-1733.e1712 (2016). https://doi.org:10.1016/j.cell.2016.11.052

30 Browder, K. C. *et al.* In vivo partial reprogramming alters age-associated molecular changes during physiological aging in mice. *Nature Aging* **2**, 243-253 (2022). https://doi.org:10.1038/s43587-022-00183-2

31 Guan, J. *et al.* Chemical reprogramming of human somatic cells to pluripotent stem cells. *Nature* **605**, 325-331 (2022). https://doi.org:10.1038/s41586-022-04593-5

32 Hou, P. *et al.* Pluripotent Stem Cells Induced from Mouse Somatic Cells by Small-Molecule Compounds. *Science* **341**, 651-654 (2013). https://doi.org:doi:10.1126/science.1239278

33 Lucas, S. *et al.* Chemical reprogramming ameliorates cellular hallmarks of aging and extends lifespan. *bioRxiv*, 2022.2008.2029.505222 (2022). https://doi.org:10.1101/2022.08.29.505222

34 Au - Khan, M. & Au - Gasser, S. Generating Primary Fibroblast Cultures from Mouse Ear and Tail Tissues. *JoVE*, e53565 (2016). https://doi.org:doi:10.3791/53565

35 Carey, B. W. *et al.* Reprogramming of murine and human somatic cells using a single polycistronic vector. *Proc Natl Acad Sci U S A* **106**, 157-162 (2009). https://doi.org:10.1073/pnas.0811426106

36 Hockemeyer, D. *et al.* A drug-inducible system for direct reprogramming of human somatic cells to pluripotency. *Cell Stem Cell* **3**, 346-353 (2008). https://doi.org:10.1016/j.stem.2008.08.014

37 Schneider, C. A., Rasband, W. S. & Eliceiri, K. W. NIH Image to ImageJ: 25 years of image analysis. *Nature Methods* **9**, 671-675 (2012). https://doi.org:10.1038/nmeth.2089

38 Arneson, A. *et al.* A mammalian methylation array for profiling methylation levels at conserved sequences. *Nature Communications* **13**, 783 (2022). https://doi.org:10.1038/s41467-022-28355-z

39 Dobin, A. *et al.* STAR: ultrafast universal RNA-seq aligner. *Bioinformatics* **29**, 15-21 (2013). https://doi.org:10.1093/bioinformatics/bts635

40 Love, M. I., Huber, W. & Anders, S. Moderated estimation of fold change and dispersion for RNA-seq data with DESeq2. *Genome Biology* **15**, 550 (2014). https://doi.org:10.1186/s13059-014-0550-8

41 Robinson, M. D., McCarthy, D. J. & Smyth, G. K. edgeR: a Bioconductor package for differential expression analysis of digital gene expression data. *Bioinformatics* **26**, 139-140 (2009). https://doi.org:10.1093/bioinformatics/btp616

42 Tyshkovskiy, A. *et al.* Identification and Application of Gene Expression Signatures Associated with Lifespan Extension. *Cell Metab* **30**, 573-593.e578 (2019). https://doi.org:10.1016/j.cmet.2019.06.018

43 Tyshkovskiy, A. *et al.* Distinct longevity mechanisms across and within species and their association with aging. *Cell* (2023). https://doi.org:https://doi.org/10.1016/j.cell.2023.05.002

44 Subramanian, A. *et al.* Gene set enrichment analysis: A knowledge-based approach for interpreting genome-wide expression profiles. *Proceedings of the National Academy of Sciences* **102**, 15545-15550 (2005). https://doi.org:doi:10.1073/pnas.0506580102

45 Shen, S. *et al.* rMATS: robust and flexible detection of differential alternative splicing from replicate RNA-Seq data. *Proc Natl Acad Sci U S A* **111**, E5593-5601 (2014). https://doi.org:10.1073/pnas.1419161111

46 Li, J. *et al.* TMTpro-18plex: The Expanded and Complete Set of TMTpro Reagents for Sample Multiplexing. *J Proteome Res* **20**, 2964-2972 (2021). https://doi.org:10.1021/acs.jproteome.1c00168

47 Navarrete-Perea, J., Yu, Q., Gygi, S. P. & Paulo, J. A. Streamlined Tandem Mass Tag (SL-TMT) Protocol: An Efficient Strategy for Quantitative (Phospho)proteome Profiling Using Tandem Mass Tag-Synchronous Precursor Selection-MS3. *J Proteome Res* **17**, 2226-2236 (2018). https://doi.org:10.1021/acs.jproteome.8b00217

48 Rappsilber, J., Ishihama, Y. & Mann, M. Stop and Go Extraction Tips for Matrix-Assisted Laser Desorption/Ionization, Nanoelectrospray, and LC/MS Sample Pretreatment in Proteomics. *Analytical Chemistry* **75**, 663-670 (2003). https://doi.org:10.1021/ac026117i

49 Paulo, J. A. *et al.* Quantitative mass spectrometry-based multiplexing compares the abundance of 5000 S. cerevisiae proteins across 10 carbon sources. *Journal of Proteomics* **148**, 85-93 (2016). https://doi.org:https://doi.org/10.1016/j.jprot.2016.07.005

50 Saba, J., Bonneil, E., Pomiès, C., Eng, K. & Thibault, P. Enhanced Sensitivity in Proteomics Experiments Using FAIMS Coupled with a Hybrid Linear Ion Trap/Orbitrap Mass Spectrometer. *Journal of Proteome Research* **8**, 3355-3366 (2009). https://doi.org:10.1021/pr801106a

51 Chambers, M. C. *et al.* A cross-platform toolkit for mass spectrometry and proteomics. *Nature Biotechnology* **30**, 918-920 (2012). https://doi.org:10.1038/nbt.2377

52 Huttlin, E. L. *et al.* A Tissue-Specific Atlas of Mouse Protein Phosphorylation and Expression. *Cell* **143**, 1174-1189 (2010). https://doi.org:https://doi.org/10.1016/j.cell.2010.12.001

53 Beausoleil, S. A., Villén, J., Gerber, S. A., Rush, J. & Gygi, S. P. A probability-based approach for high-throughput protein phosphorylation analysis and site localization. *Nature Biotechnology* **24**, 1285-1292 (2006). https://doi.org:10.1038/nbt1240

54 Elias, J. E. & Gygi, S. P. Target-decoy search strategy for increased confidence in large-scale protein identifications by mass spectrometry. *Nature Methods* **4**, 207-214 (2007). https://doi.org:10.1038/nmeth1019

55 McAlister, G. C. *et al.* Increasing the Multiplexing Capacity of TMTs Using Reporter Ion Isotopologues with Isobaric Masses. *Analytical Chemistry* **84**, 7469-7478 (2012). https://doi.org:10.1021/ac301572t

56 Goeminne, L. J. E., Gevaert, K. & Clement, L. Experimental design and data-analysis in label-free quantitative LC/MS proteomics: A tutorial with MSqRob. *J Proteomics* **171**, 23-36 (2018). https://doi.org:10.1016/j.jprot.2017.04.004

57 Goeminne, L. J., Gevaert, K. & Clement, L. Peptide-level Robust Ridge Regression Improves Estimation, Sensitivity, and Specificity in Data-dependent Quantitative Label-free Shotgun Proteomics. *Mol Cell Proteomics* **15**, 657-668 (2016). https://doi.org:10.1074/mcp.M115.055897

58 Hornbeck, P. V. *et al.* PhosphoSitePlus, 2014: mutations, PTMs and recalibrations. *Nucleic Acids Research* **43**, D512-D520 (2014). https://doi.org:10.1093/nar/gku1267

59 Divakaruni, A. S., Paradyse, A., Ferrick, D. A., Murphy, A. N. & Jastroch, M. Analysis and interpretation of microplate-based oxygen consumption and pH data. *Methods Enzymol* **547**, 309-354 (2014). https://doi.org:10.1016/b978-0-12-801415-8.00016-3

60 Rojas-Tapias, D. F. *et al.* Inflammation-associated nitrate facilitates ectopic colonization of oral bacterium Veillonella parvula in the intestine. *Nature Microbiology* **7**, 1673-1685 (2022). https://doi.org:10.1038/s41564-022-01224-7

61 Sturm, G. *et al.* Human aging DNA methylation signatures are conserved but accelerated in cultured fibroblasts. *Epigenetics* **14**, 961-976 (2019). https://doi.org:10.1080/15592294.2019.1626651

62 Campbell, P. A. Alkaline Phosphatase Staining. *Bio-protocol* **4**, e1060 (2014). https://doi.org:10.21769/BioProtoc.1060

63 Hagen, T. M. *et al.* Mitochondrial decay in hepatocytes from old rats: Membrane potential declines, heterogeneity and oxidants increase. *Proceedings of the National Academy of Sciences* **94**, 3064-3069 (1997). https://doi.org:doi:10.1073/pnas.94.7.3064

64 Berry, B. J. *et al.* Preservation of mitochondrial membrane potential is necessary for lifespan extension from dietary restriction. *Geroscience* (2023). https://doi.org:10.1007/s11357-023-00766-w

65 Berry, B. J. *et al.* Optogenetic rejuvenation of mitochondrial membrane potential extends C. elegans lifespan. *Nature Aging* **3**, 157-161 (2023). https://doi.org:10.1038/s43587-022-00340-7

66 Shi, G. *et al.* Bend family proteins mark chromatin boundaries and synergistically promote early germ cell differentiation. *Protein Cell* **13**, 721-741 (2022). https://doi.org:10.1007/s13238-021-00884-1

67 Sevilla, A. *et al.* An Esrrb and Nanog Cell Fate Regulatory Module Controlled by Feed Forward Loop Interactions. *Frontiers in Cell and Developmental Biology* **9** (2021). https://doi.org:10.3389/fcell.2021.630067

68 Lowry, W. E. *et al.* Generation of human induced pluripotent stem cells from dermal fibroblasts. *Proceedings of the National Academy of Sciences* **105**, 2883-2888 (2008). https://doi.org:doi:10.1073/pnas.0711983105

69 Takahashi, K. & Yamanaka, S. Induction of pluripotent stem cells from mouse embryonic and adult fibroblast cultures by defined factors. *Cell* **126**, 663-676 (2006). https://doi.org:10.1016/j.cell.2006.07.024

70 Gladyshev, V. N. *et al.* Molecular Damage in Aging. *Nat Aging* **1**, 1096-1106 (2021). https://doi.org:10.1038/s43587-021-00150-3

71 Covelo-Molares, H., Bartosovic, M. & Vanacova, S. RNA methylation in nuclear pre-mRNA processing. *Wiley Interdiscip Rev RNA* **9**, e1489 (2018). https://doi.org:10.1002/wrna.1489

72 Sóti, C. & Csermely, P. Molecular chaperones and the aging process. *Biogerontology* **1**, 225-233 (2000). https://doi.org:10.1023/a:1010082129022

73 Ewald, C. Y. The Matrisome during Aging and Longevity: A Systems-Level Approach toward Defining Matreotypes Promoting Healthy Aging. *Gerontology* **66**, 266-274 (2020). https://doi.org:10.1159/000504295

74 Shpilka, T. & Haynes, C. M. The mitochondrial UPR: mechanisms, physiological functions and implications in ageing. *Nature Reviews Molecular Cell Biology* **19**, 109-120 (2018). https://doi.org:10.1038/nrm.2017.110

75 Turnham, R. E. & Scott, J. D. Protein kinase A catalytic subunit isoform PRKACA; History, function and physiology. *Gene* **577**, 101-108 (2016). https://doi.org:10.1016/j.gene.2015.11.052

76 Zhang, L. *et al.* Role of the Balance of Akt and MAPK Pathways in the Exercise-Regulated Phenotype Switching in Spontaneously Hypertensive Rats. *Int J Mol Sci* **20** (2019). https://doi.org:10.3390/ijms20225690

77 Paynter, N. P. *et al.* Metabolic Predictors of Incident Coronary Heart Disease in Women. *Circulation* **137**, 841-853 (2018). https://doi.org:10.1161/circulationaha.117.029468

78 Poganik, J. R. *et al.* Biological age is increased by stress and restored upon recovery. *Cell Metabolism* **35**, 807-820.e805 (2023). https://doi.org:https://doi.org/10.1016/j.cmet.2023.03.015

79 Lin, C. C., Chen, Y. P., Yang, W. Z., Shen, J. C. K. & Yuan, H. S. Structural insights into CpG-specific DNA methylation by human DNA methyltransferase 3B. *Nucleic Acids Res* **48**, 3949-3961 (2020). https://doi.org:10.1093/nar/gkaa111

80 Kumar, R., Srivastava, R., Singh, R. K., Surolia, A. & Rao, D. N. Activation and inhibition of DNA methyltransferases by S-adenosyl-L-homocysteine analogues. *Bioorg Med Chem* **16**, 2276-2285 (2008). https://doi.org:10.1016/j.bmc.2007.11.075

81 McBreairty, L. E., Robinson, J. L., Furlong, K. R., Brunton, J. A. & Bertolo, R. F. Guanidinoacetate is more effective than creatine at enhancing tissue creatine stores while consequently limiting methionine availability in Yucatan miniature pigs. *PLoS One* **10**, e0131563 (2015). https://doi.org:10.1371/journal.pone.0131563

82 Wharton, W. & Goz, B. The inhibition by xanthine phosphodiesterase inhibitors of the induction of alkaline phosphatase activity in HeLa cells: Relationship of enzyme activity to cyclic AMP

concentrations. *Journal of Cellular Physiology* **100**, 509-518 (1979). https://doi.org:https://doi.org/10.1002/jcp.1041000313

83 Panyard, D. J., Yu, B. & Snyder, M. P. The metabolomics of human aging: Advances, challenges, and opportunities. *Science Advances* **8**, eadd6155 https://doi.org:10.1126/sciadv.add6155

84 Maffei, M. E. 5-Hydroxytryptophan (5-HTP): Natural Occurrence, Analysis, Biosynthesis, Biotechnology, Physiology and Toxicology. *Int J Mol Sci* **22** (2020). https://doi.org:10.3390/ijms22010181

85 Fukuwatari, T. & Shibata, K. Effect of nicotinamide administration on the tryptophan-nicotinamide pathway in humans. *Int J Vitam Nutr Res* **77**, 255-262 (2007). https://doi.org:10.1024/0300-9831.77.4.255

86 Yamauchi, M. & Sricholpech, M. Lysine post-translational modifications of collagen. *Essays Biochem* **52**, 113-133 (2012). https://doi.org:10.1042/bse0520113

87 Mozhui, K. *et al.* Genetic loci and metabolic states associated with murine epigenetic aging. *eLife* **11**, e75244 (2022). https://doi.org:10.7554/eLife.75244

88 Nishimura, K., Fukuda, A. & Hisatake, K. Mechanisms of the Metabolic Shift during Somatic Cell Reprogramming. *Int J Mol Sci* **20** (2019). https://doi.org:10.3390/ijms20092254

89 Brandt, T. *et al.* Changes of mitochondrial ultrastructure and function during ageing in mice and Drosophila. *eLife* **6**, e24662 (2017). https://doi.org:10.7554/eLife.24662

90 Lu, X. *et al.* Ultrastructural and proteomic profiling of mitochondria-associated endoplasmic reticulum membranes reveal aging signatures in striated muscle. *Cell Death & Disease* **13**, 296 (2022). https://doi.org:10.1038/s41419-022-04746-4

91 Katharine, E. S. *et al.* Age-Related Changes in Axonal and Mitochondrial Ultrastructure and Function in White Matter. *The Journal of Neuroscience* **36**, 9990 (2016). https://doi.org:10.1523/JNEUROSCI.1316-16.2016

92 Warnsmann, V. *et al.* Disruption of the MICOS complex leads to an aberrant cristae structure and an unexpected, pronounced lifespan extension in Podospora anserina. *J Cell Biochem* **123**, 1306-1326 (2022). https://doi.org:10.1002/jcb.30278

93 Zer, V. *et al.* Tri-dimensional Mitochondria Reconstructions of Cardiac Muscle Changes in Size Across Aging due to the MICOS Complex. *bioRxiv*, 2022.2004.2023.489291 (2022). https://doi.org:10.1101/2022.04.23.489291

94 Pellegrini, L. & Scorrano, L. A cut short to death: Parl and Opa1 in the regulation of mitochondrial morphology and apoptosis. *Cell Death & Differentiation* **14**, 1275-1284 (2007). https://doi.org:10.1038/sj.cdd.4402145

95 Sharma, A., Smith, H. J., Yao, P. & Mair, W. B. Causal roles of mitochondrial dynamics in longevity and healthy aging. *EMBO Rep* **20**, e48395 (2019). https://doi.org:10.15252/embr.201948395

96 Rana, A. *et al.* Promoting Drp1-mediated mitochondrial fission in midlife prolongs healthy lifespan of Drosophila melanogaster. *Nature Communications* **8**, 448 (2017). https://doi.org:10.1038/s41467-017-00525-4

97 Semba, R. D., Moaddel, R., Zhang, P., Ramsden, C. E. & Ferrucci, L. Tetra-linoleoyl cardiolipin depletion plays a major role in the pathogenesis of sarcopenia. *Med Hypotheses* **127**, 142-149 (2019). https://doi.org:10.1016/j.mehy.2019.04.015

98 Daum, B., Walter, A., Horst, A., Osiewacz, H. D. & Kühlbrandt, W. Age-dependent dissociation of ATP synthase dimers and loss of inner-membrane cristae in mitochondria. *Proceedings of the National Academy of Sciences* **110**, 15301-15306 (2013). https://doi.org:doi:10.1073/pnas.1305462110

99 Rottenberg, H. & Hoek, J. B. The Mitochondrial Permeability Transition: Nexus of Aging, Disease and Longevity. *Cells* **10** (2021). https://doi.org:10.3390/cells10010079

100 Angeli, S. *et al.* The mitochondrial permeability transition pore activates the mitochondrial unfolded protein response and promotes aging. *eLife* **10**, e63453 (2021). https://doi.org:10.7554/eLife.63453

101 Sun, N., Youle, R. J. & Finkel, T. The Mitochondrial Basis of Aging. *Mol Cell* **61**, 654-666 (2016). https://doi.org:10.1016/j.molcel.2016.01.028

102 Gómez, L. A. & Hagen, T. M. Age-related decline in mitochondrial bioenergetics: does supercomplex destabilization determine lower oxidative capacity and higher superoxide production? *Semin Cell Dev Biol* **23**, 758-767 (2012). https://doi.org:10.1016/j.semcdb.2012.04.002

103 Zhang, H. *et al.* Reduction of elevated proton leak rejuvenates mitochondria in the aged cardiomyocyte. *Elife* **9** (2020). https://doi.org:10.7554/eLife.60827

104 Novack, G. V., Galeano, P., Castaño, E. M. & Morelli, L. Mitochondrial Supercomplexes: Physiological Organization and Dysregulation in Age-Related Neurodegenerative Disorders. *Front Endocrinol (Lausanne)* **11**, 600 (2020). https://doi.org:10.3389/fendo.2020.00600

105 Patron, M. *et al.* Regulation of mitochondrial proteostasis by the proton gradient. *The EMBO Journal* **41**, e110476 (2022). https://doi.org:https://doi.org/10.15252/embj.2021110476

106 Moehle, E. A., Shen, K. & Dillin, A. Mitochondrial proteostasis in the context of cellular and organismal health and aging. *J Biol Chem* **294**, 5396-5407 (2019). https://doi.org:10.1074/jbc.TM117.000893

107 Enns, L. C., Pettan-Brewer, C. & Ladiges, W. Protein kinase A is a target for aging and the aging heart. *Aging (Albany NY)* **2**, 238-243 (2010). https://doi.org:10.18632/aging.100138

108 Enns, L. C. & Ladiges, W. Protein kinase A signaling as an anti-aging target. *Ageing Res Rev* **9**, 269-272 (2010). https://doi.org:10.1016/j.arr.2010.02.004

109 Dagda, R. K. & Das Banerjee, T. Role of protein kinase A in regulating mitochondrial function and neuronal development: implications to neurodegenerative diseases. *Rev Neurosci* **26**, 359-370 (2015). https://doi.org:10.1515/revneuro-2014-0085

110 Lark, D. S. *et al.* Protein Kinase A Governs Oxidative Phosphorylation Kinetics and Oxidant Emitting Potential at Complex I. *Frontiers in Physiology* **6** (2015). https://doi.org:10.3389/fphys.2015.00332

111 Enns, L. C. *et al.* Disruption of Protein Kinase A in Mice Enhances Healthy Aging. *PLOS ONE* **4**, e5963 (2009). https://doi.org:10.1371/journal.pone.0005963

112 Hothorn, T., Bretz, F. & Westfall, P. Simultaneous inference in general parametric models. *Biom J* **50**, 346-363 (2008). https://doi.org:10.1002/bimj.200810425

113 Xia, J., Psychogios, N., Young, N. & Wishart, D. S. MetaboAnalyst: a web server for metabolomic data analysis and interpretation. *Nucleic Acids Research* **37**, W652-W660 (2009). https://doi.org:10.1093/nar/gkp356

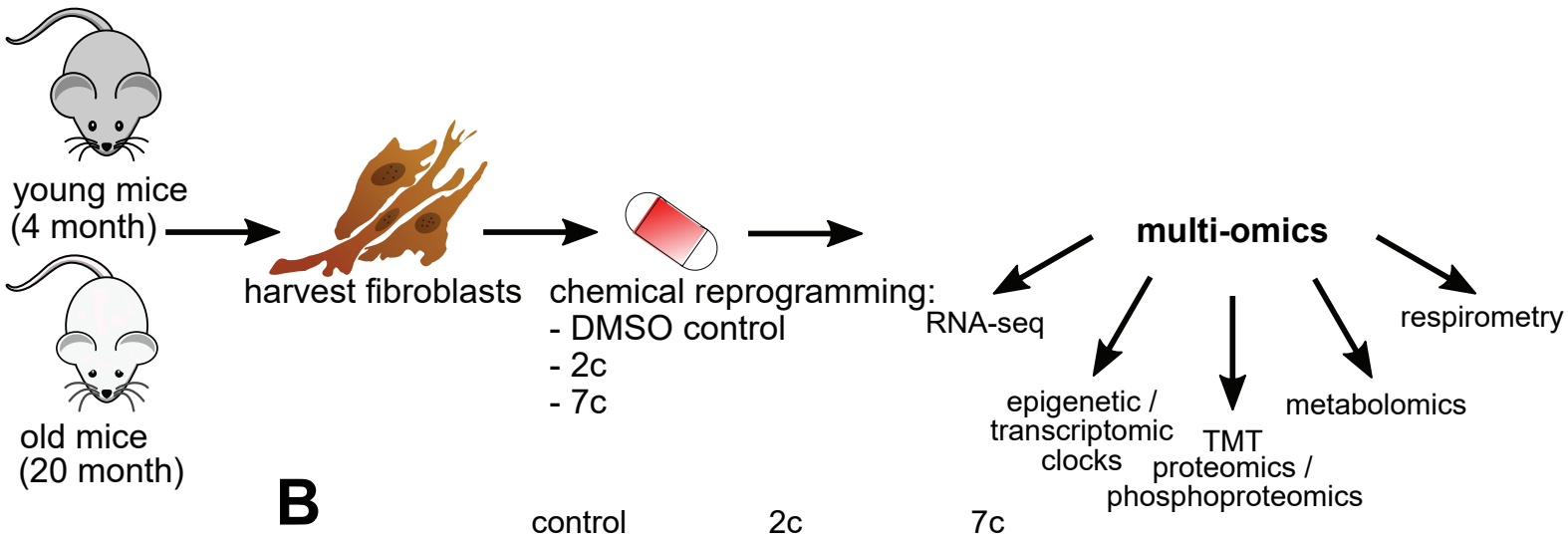

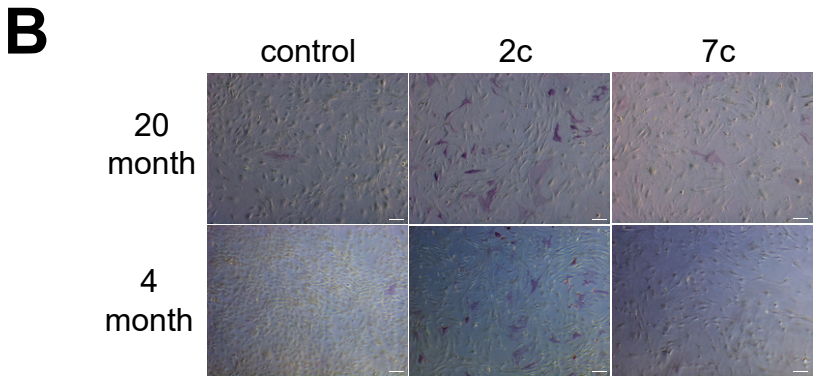

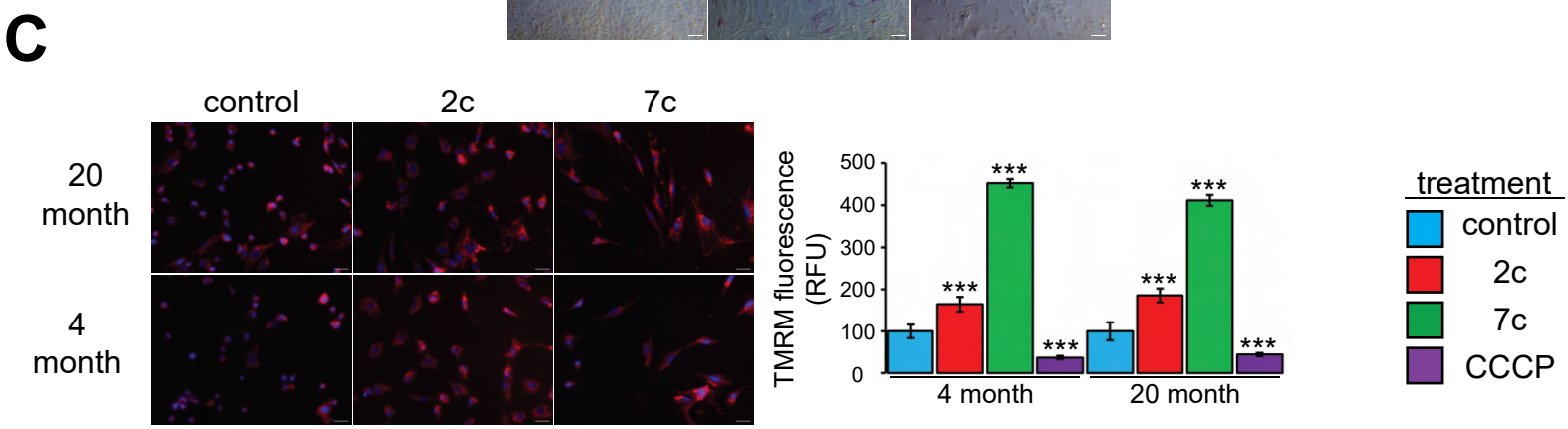

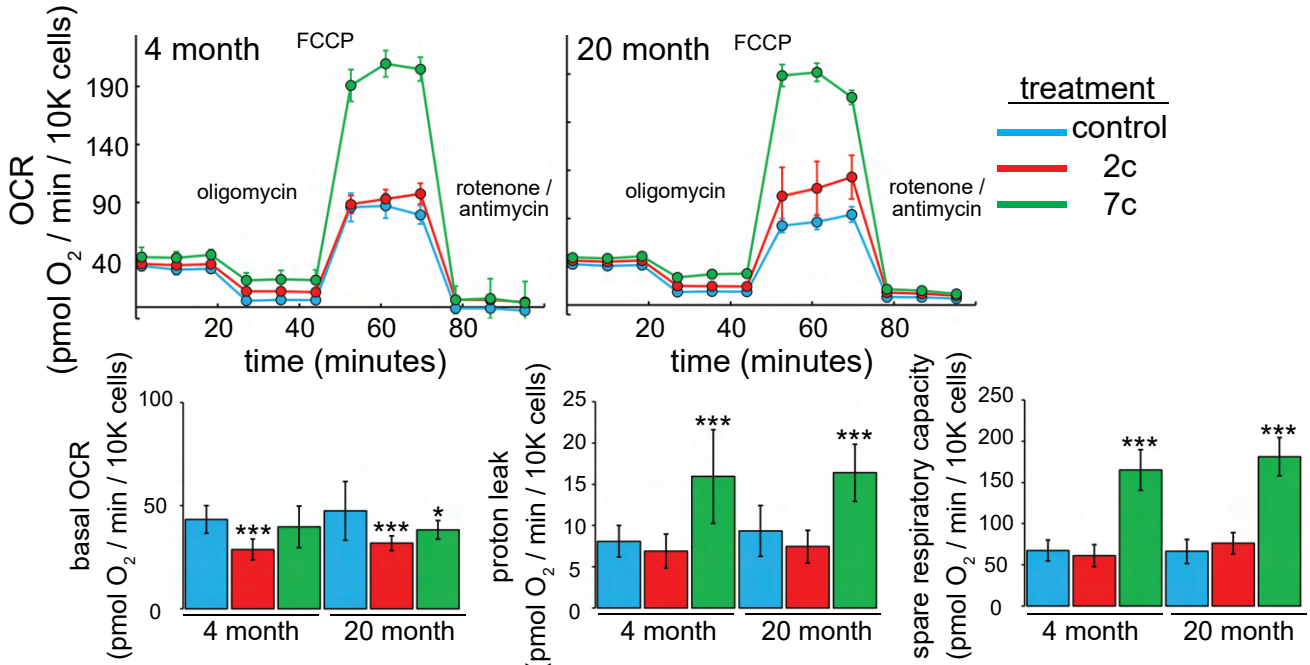

Figure 1

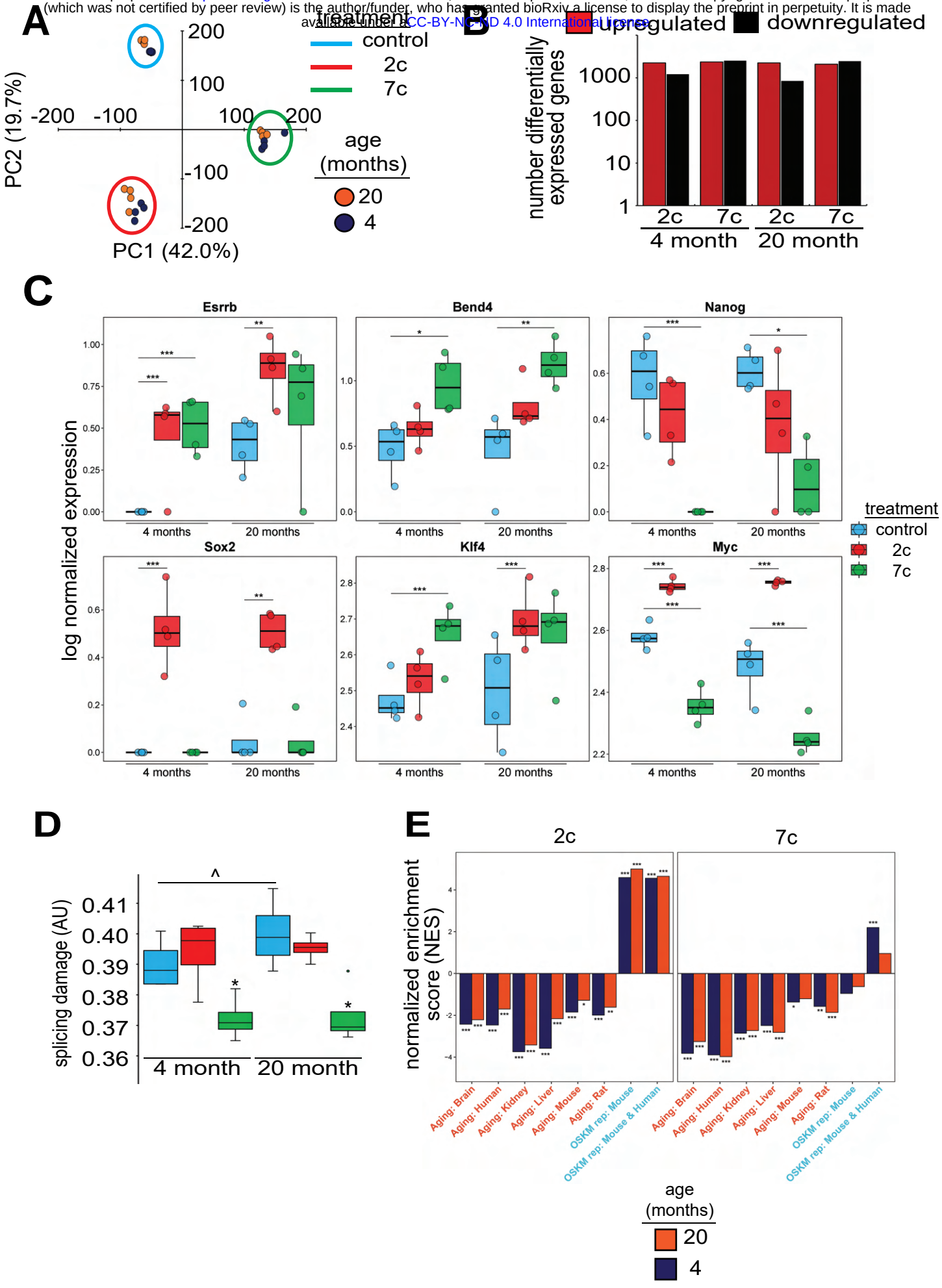

Figure 2

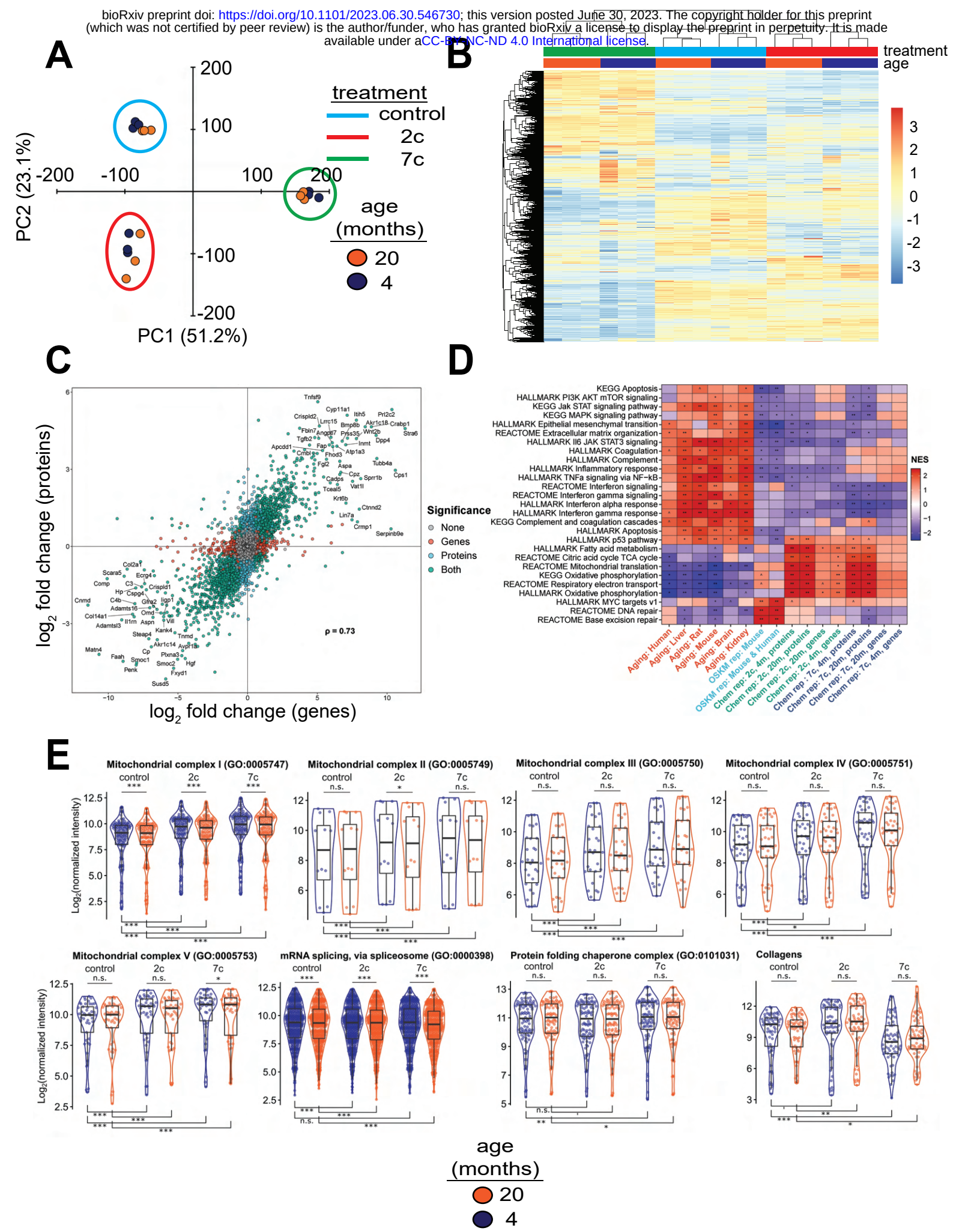

Figure 3

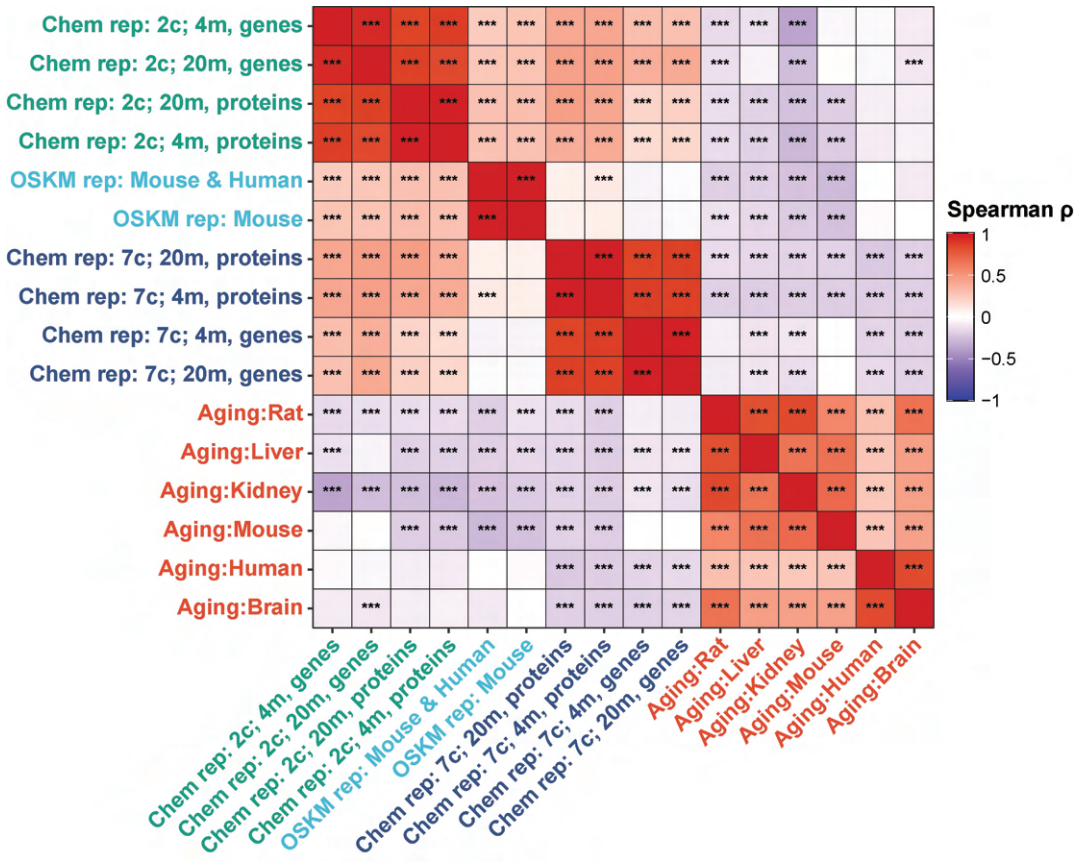

Figure 4

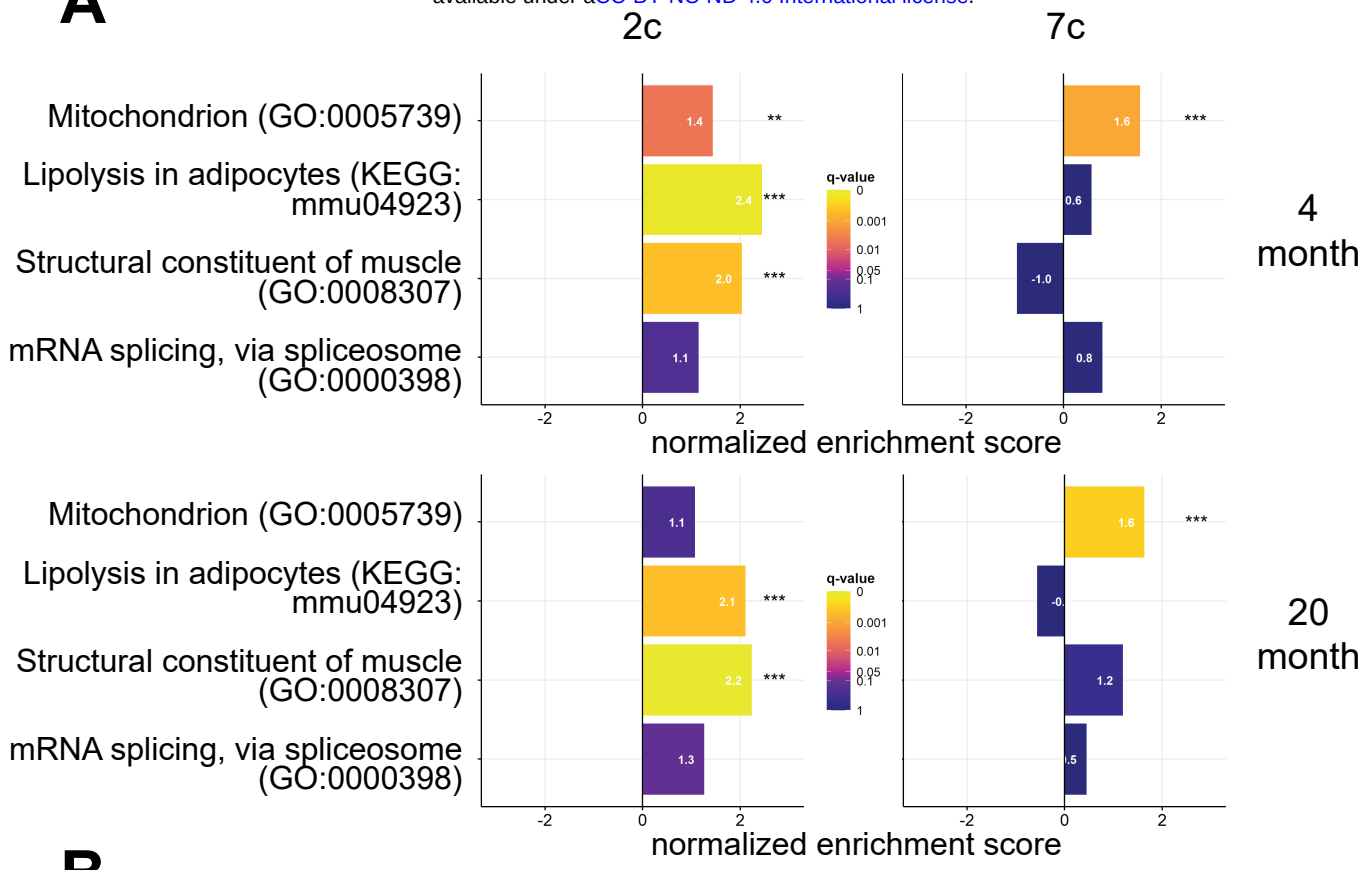

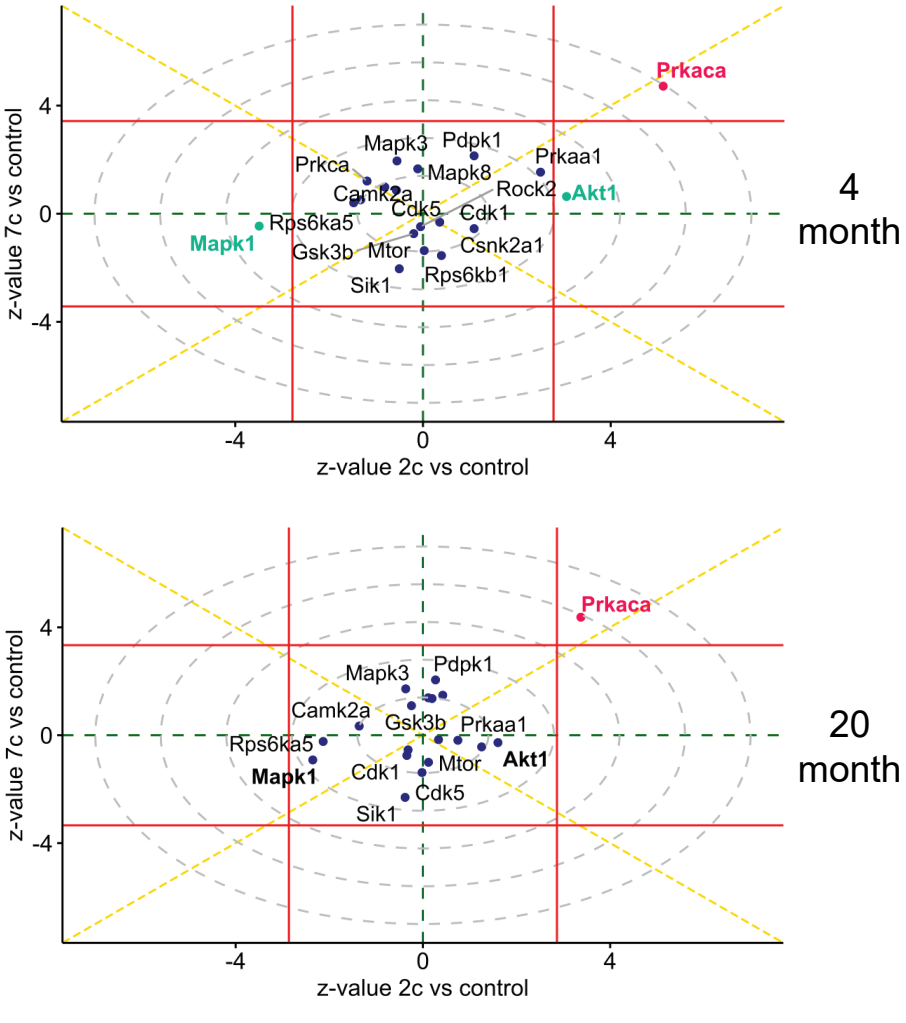

Figure 5

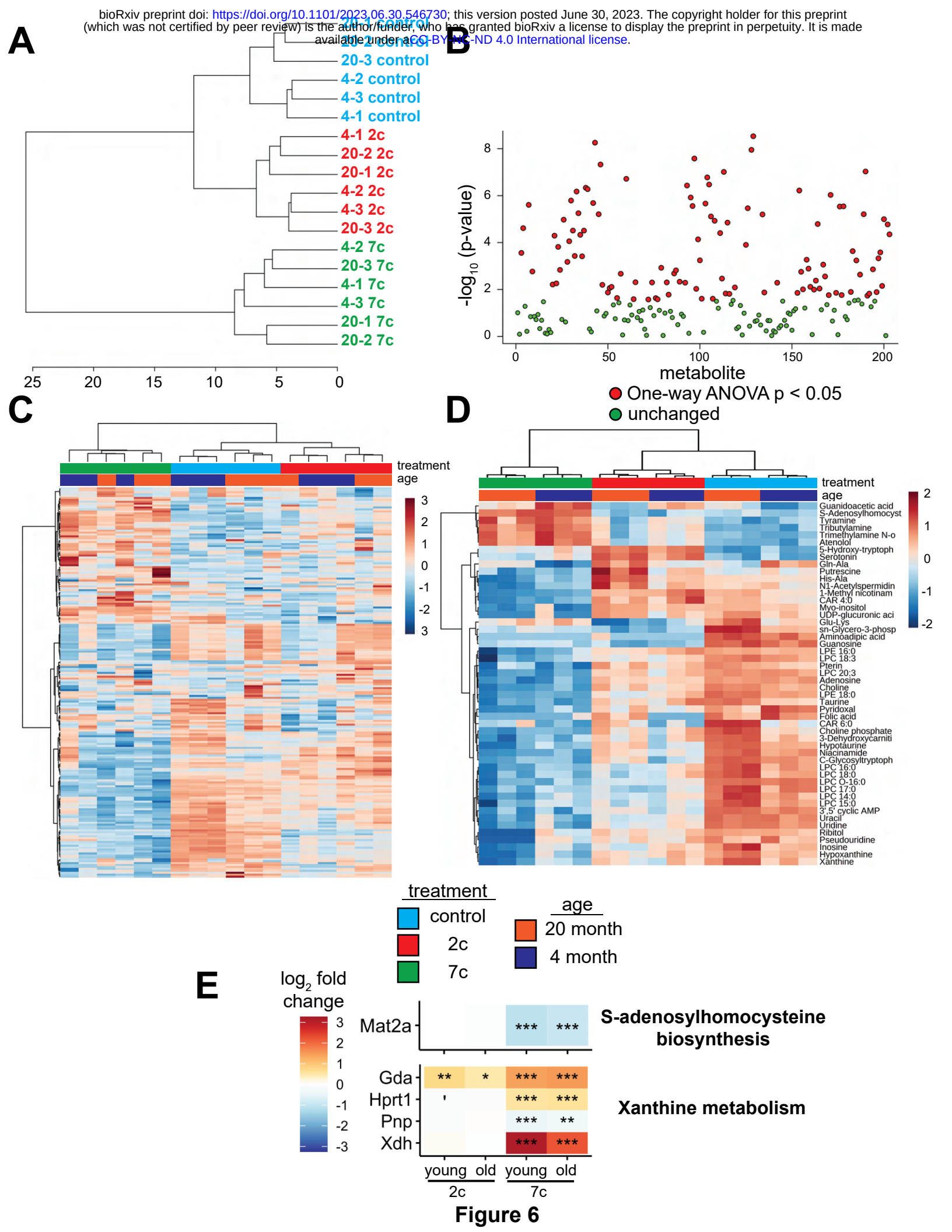

Figure 6

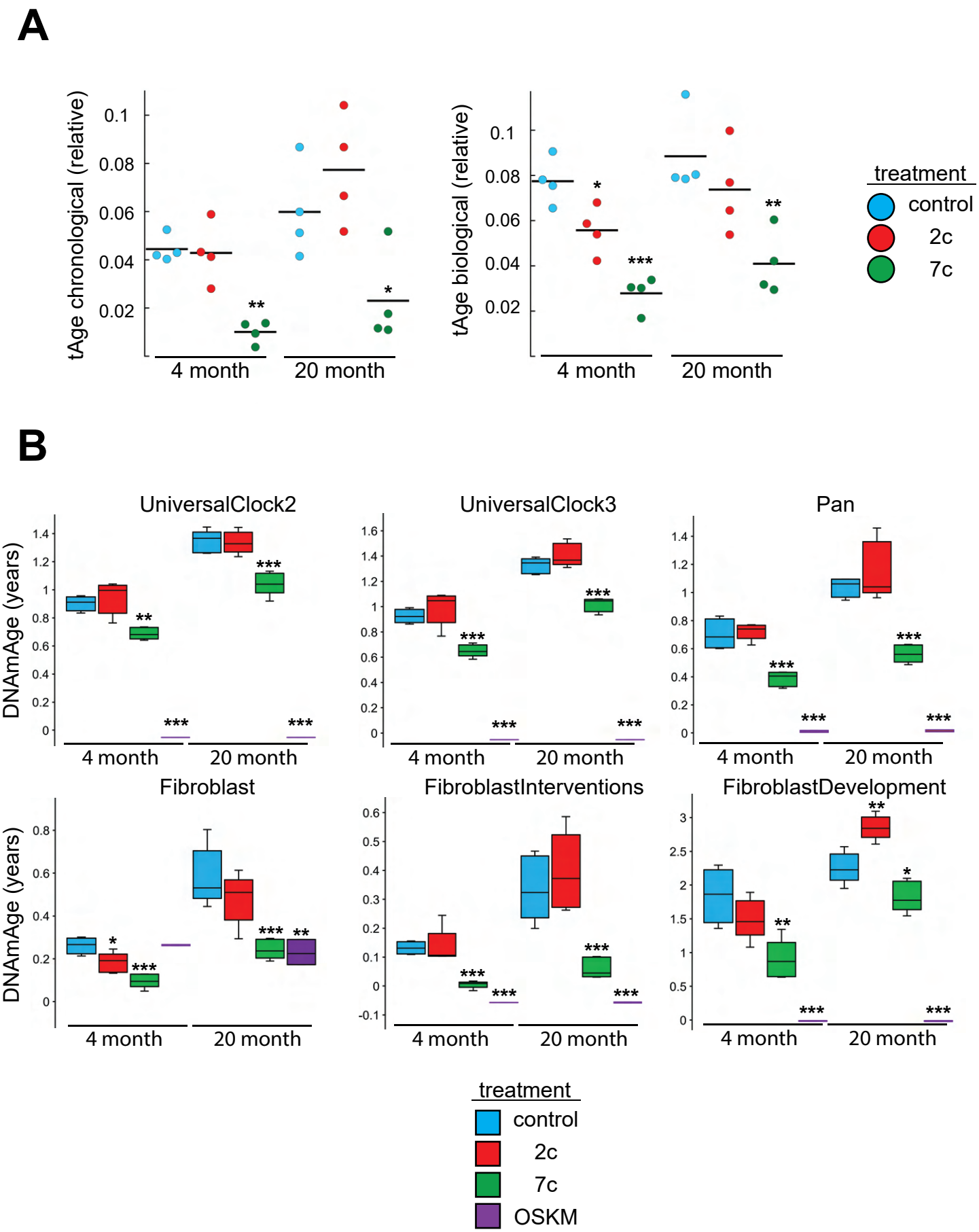

Figure 7